NASA/TM–20230001411

A regression analysis of measured and modeled sonic booms across a lateral microphone array

J. Taggart Durrant
Brigham Young University, Provo, Utah

William J. Doebler, Alexandra Loubeau, Aaron B. Vaughn
Langley Research Center, Hampton, Virginia

Kent L. Gee
Brigham Young University, Provo, Utah

March 2025

NASA STI Program Report Series

Since its founding, NASA has been dedicated to the advancement of aeronautics and space science. The NASA scientific and technical information (STI) program plays a key part in helping NASA maintain this important role.

The NASA STI program operates under the auspices of the Agency Chief Information Officer. It collects, organizes, provides for archiving, and disseminates NASA's STI. The NASA STI program provides access to the NTRS Registered and its public interface, the NASA Technical Reports Server, thus providing one of the largest collections of aeronautical and space science STI in the world. Results are published in both non-NASA channels and by NASA in the NASA STI Report Series, which includes the following report types:

- TECHNICAL PUBLICATION. Reports of completed research or a major significant phase of research that present the results of NASA Programs and include extensive data or theoretical analysis. Includes compilations of significant scientific and technical data and information deemed to be of continuing reference value. NASA counterpart of peer-reviewed formal professional papers but has less stringent limitations on manuscript length and extent of graphic presentations.

- TECHNICAL MEMORANDUM. Scientific and technical findings that are preliminary or of specialized interest, e.g., quick release reports, working papers, and bibliographies that contain minimal annotation. Does not contain extensive analysis.

- CONTRACTOR REPORT. Scientific and technical findings by NASA-sponsored contractors and grantees.

- CONFERENCE PUBLICATION. Collected papers from scientific and technical conferences, symposia, seminars, or other meetings sponsored or co-sponsored by NASA.

- SPECIAL PUBLICATION. Scientific, technical, or historical information from NASA programs, projects, and missions, often concerned with subjects having substantial public interest.

- TECHNICAL TRANSLATION. English-language translations of foreign scientific and technical material pertinent to NASA's mission.

Specialized services also include organizing and publishing research results, distributing specialized research announcements and feeds, providing information desk and personal search support, and enabling data exchange services.

For more information about the NASA STI program, see the following:

- Access the NASA STI program home page at http://www.sti.nasa.gov

- Help desk contact information:

https://www.sti.nasa.gov/sti-contact-form/
and select the "General" help request type.

NASA/TM–20230001411

A regression analysis of measured and modeled sonic booms across a lateral microphone array

J. Taggart Durrant
Brigham Young University, Provo, Utah

William J. Doebler, Alexandra Loubeau, Aaron B. Vaughn
Langley Research Center, Hampton, Virginia

Kent L. Gee
Brigham Young University, Provo, Utah

National Aeronautics and
Space Administration

Langley Research Center
Hampton, Virginia 23681-2199

March 2025

Available from:

NASA STI Program / Mail Stop 050
NASA Langley Research Center
Hampton, VA 23681-2199

Table of contents page

Table of figures

Table of tables

Nomenclature and acronyms

ASEL	A-weighted Sound Exposure Level
BSEL	B-weighted Sound Exposure Level
BYU	Brigham Young University
CarpetDIEM	Carpet Determination in Entirety Measurement
CFD	Computational Fluid Dynamics
CFSv2	Climate Forecast System version 2
DSEL	D-weighted Sound Exposure Level
ESEL	E-weighted Sound Exposure Level
FPA	Flight Path Angle
ISBAP	Indoor Sonic Boom Annoyance Predictor
Lasso	Least Absolute Shrinkage and Selection Operator
LSQ	Ordinary least squares multiple linear regression
MSE	Mean Squared Error
OTO	One-third octave band
PL	Perceived Level
ΔPM	Predicted minus measured metric value
$\Delta\mathrm{PM}_{\mathrm{PL}}$	Predicted minus measured PL value
QSF18	Quiet Supersonic Flights 2018
RMSE	Root Mean Square Error
ROM	Reduced-Order Model
R/L	Radius of propagation starting point over the Length of the aircraft
SD	Standard Deviation
SE	Standard Error
SNR	Signal-to-Noise Ratio
Volpe	United States Department of Transportation John A. Volpe National Transportation Systems Center

Abstract

This memorandum demonstrates least absolute shrinkage and selection operator (Lasso) regression and compares results with modeled and measured sonic boom data. The data are from the NASA Carpet Determination In Entirety Measurement Phase I (CarpetDIEM I) test flight campaign with an F/A-18 A aircraft. Sonic boom predictions are modeled using PCBoom and compared with ground-based field measurements. Lasso regression identifies the relative contributions of 68 parameters to the prediction variability. A reduced-order model (ROM) can be implemented using a smaller subset of the most significant parameters to improve predictions. The results of these regression analyses can help guide future efforts to improve sonic boom predictions. Overall, this work provides a framework for implementing Lasso regression to identify sources of sonic boom measurement variability and prediction misestimation.

I. INTRODUCTION

Correct predictions of sonic boom levels are important for assessing the potential noise impact of commercial supersonic aviation and reusable rockets. NASA is preparing to fly the X-59 aircraft over communities to collect data on the general public's response to noise from en-route supersonic flight as part of its Quesst mission (Rathsam et al., 2023). The collected community response data will inform regulators as they reassess the ban on overland commercial supersonic flight, potentially opening a new sector in the aviation industry. Another source of sonic booms are reusable rockets, such as Space X's Falcon 9, which create a sonic boom upon reentry and are launching in increasing cadence (Durrant et al., 2022c). These supersonic endeavors rely on level predictions to assess their potential noise impact.

NASA developed a suite of sonic boom prediction tools known as PCBoom (Page et al., 2010). Continual enhancements are made to PCBoom to improve its functionality and accuracy (Lonzaga et al., 2022a). Previous measurement campaigns have shown high variability in levels of sonic boom perception metrics, even between ground microphone stations within a few hundred feet of each other (Durrant et al., 2022a). Metric variability arises from many factors, including the varying atmosphere, aircraft trajectory, and ambient environment. It is important to understand the variation in sonic boom metrics at the ground due to these and other factors to improve the accuracy of PCBoom predictions and to analyze the measured acoustic data.

Regression analysis can help identify sources of variability and differences between measurements and predictions. Least absolute shrinkage and selection operator (Lasso) regression was previously applied to sonic boom data from a supersonic flight campaign (Quiet Supersonic Flights 2018, see Appendix A for more details). The sonic booms were generated using a low-boom dive maneuver. Lasso identified the nine most significant contributors from meteorological, aircraft trajectory, and ambient factors for predicting sonic boom levels. From these nine factors, an ordinary least squares multiple linear regression (LSQ) was performed to create a reduced order model (ROM). This model better accounts for the variability in the boom metrics than PCBoom predictions alone.

The present work demonstrates and applies Lasso regression to data from a NASA test flight campaign, Carpet Determination In Entirety Measurement Phase I (CarpetDIEM I). This dataset is more representative of future supersonic endeavors with steady, level overflights instead of the low-boom dive maneuver that was analyzed in previous work. First, Section II provides an overview of CarpetDIEM I measurements. Section III describes PCBoom predictions and compares them with measured sonic booms from CarpetDIEM I. Section IV demonstrates Lasso regression to identify and investigate factors that explain both measured levels and differences between PCBoom predictions and measurements. Additionally, Section IV explores the efficacy of using an LSQ-regression-based ROM as a potential empirical aid to PCBoom predictions. Lastly, Section V summarizes the paper and offers concluding remarks.

II. CARPETDIEM I MEASUREMENT OVERVIEW

NASA conducted the CarpetDIEM I flight test campaign to prepare for the logistics and operations of future acoustic validation with the X-59 aircraft. The test took place east of Edwards Air Force Base in California in the summer of 2019. There were 23 supersonic overflights over 3 days from an F/A-18 A aircraft flying perpendicular to an array of microphones. Altitude and Mach number were nominally the same for each flight. Each flight had four steady, level supersonic passes over the array, except one had three. This test setup is expected to resemble a subset of the Quesst Phase 2 Acoustic Validation test with the X-59 aircraft. This makes the CarpetDIEM I data useful for applying Lasso regression and developing a framework to analyze future sonic boom data.

Figure 1 shows measurement sites and an example trajectory map from CarpetDIEM I. The measurement sites were numbered 1 to 71, where site 1 is on the northernmost end of the array (+Y) and site 71 is on the southernmost end (−Y). The trajectory is nominally perpendicular to the array and centered over site 36 (noted in green).

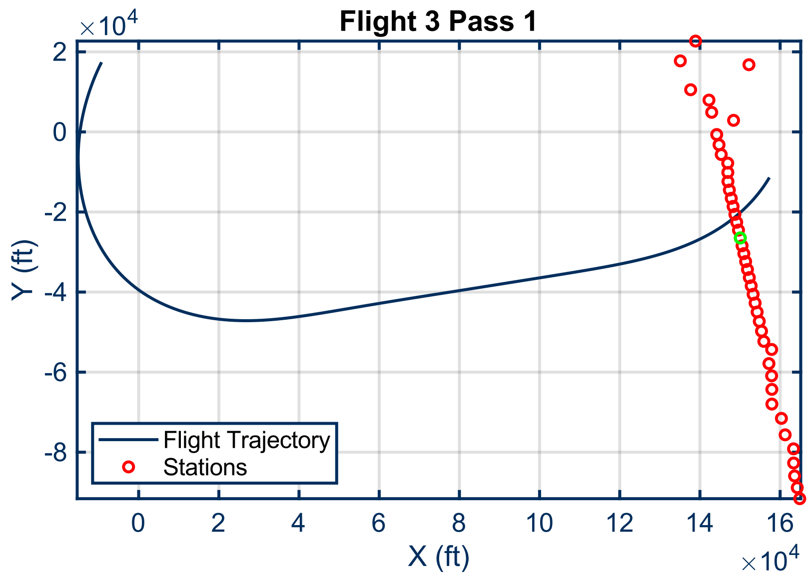

Figure 1. The F/A-18 flight trajectory (from left to right) for the first pass during the third flight as indicated by a solid line. The 71 ground measurement sites are shown as red circles with a green circle at site 36.

The average and standard deviation (SD) of measured noise levels from CarpetDIEM I provide insight into the amount of measured variability. Table 1 gives the average and SD computed over all booms and all measurement stations for each of the six candidate metrics for en-route supersonic aircraft noise certification (Page and Loubeau, 2019). The measured booms were trimmed to a 650 ms window with 100 ms before the first shock. Corrections for ambient noise were applied which did not affect the results due to a high signal-to-noise ratio in the quiet environment.

Table 1. Average and standard deviation of metric levels over all booms at all stations.

Metric:	**PL**	**ASEL**	**BSEL**	**DSEL**	**ESEL**	**ISBAP**
Average value (dB):	98.7	83.6	93.8	94.1	90.7	107.2
Standard Deviation (dB):	7.4	7.7	5.8	5.5	6.4	6.1

While propagation distance from the aircraft is known to contribute to variability, there appear to be other factors. Focusing on the results in Perceived Level (PL) (Stevens, 1972), the SD over all booms and attended stations[1] was 7.4 dB. Even though the altitude and Mach number were nominally the same for each flight, the measurements at the same station differed significantly from boom to boom. For example, the SD of the 23 measured PL values at the center of the array (site 36) is similar to that towards the southern edge (site 54) at 5.7 dB and 5.3 dB, respectively. Thus, factors other than propagation distance likely contribute to measured variability.

III. PCBOOM PREDICTIONS

This section compares PCBoom predictions and CarpetDIEM I measurements of sonic boom waveforms, peak pressures, and perception metrics. Data from CarpetDIEM I provide an opportunity to assess the effectiveness and accuracy of the Enhanced Burgers module from PCBoom 7.2 (Page et al., 2020c). When analyzing PCBoom accuracy, the measured metrics are assumed to be known without error and considered the “truth” for comparing with predictions. Effects of near-field input choices are also studied by comparing waveforms generated from the PCBoom built-in F/A-18 F-function near-field and computational fluid dynamics (CFD) near-field pressure signatures described in this section.

A. PCBoom Prediction Description

PCBoom waveforms and the associated metrics were computed for each station and boom. Predictions were computed using a two-step process: 1) determine the ray location for each measurement location and 2) propagate the near field to determine the waveform at the ground.

For the first step, the PCBoom Enhanced Burgers module was run in “footprint” mode, which generates a footprint of the ray landing positions for each pass. From these, the ray that arrives at each microphone site can be determined. Each footprint was generated assuming a flat earth (SCHULFLAT ray tracing mode) with 1-degree azimuthal ray launch resolution. The mismatch between the flat earth mode and the varying terrain required multiple PCBoom footprint runs of each pass, with each run having a different ground elevation to match the elevation of each microphone site.[2] The elevation of each site was determined using Google Earth Pro, which has a roadway elevation mean absolute error of 1.32 m (Wang et al., 2017). The elevation varies by almost 200 m (656 ft) across the 71 measurement sites.

For the second step, the PCBoom Enhanced Burgers module was run in “waveform” mode for each of the rays that land at the microphone sites. The perception metrics were computed for the ground waveforms after applying a ground reflection factor of 1.9 to the free-field pressure. This ground reflection factor corresponds to hard ground and previously showed good agreement between experiment and theoretical data from a sonic boom study in Oklahoma City (Carlson et al, 1966). Two sets of ground waveforms were generated for each pass using two near-field sources, F-function and CFD, which are described hereafter.

---

[1] Prior to CarpetDIEM I, a set of geographical sites were approved by the Bureau of Land Management (BLM) for a large flight-track perpendicular microphone array to be used for the Quesst mission Phase 2: Acoustic Validation. However, as CarpetDIEM I was a pre-test, not all BLM-approved sites were instrumented each day. Instead, acoustic pressure corresponding to rays of specific azimuthal emission angles were attempted to be measured each day, and the limited set of microphones were moved to different positions to capture them based on the weather of the day.

[2] There is a TERRAIN keyword in PCBoom that was not used because its algorithm may underestimate the carpet edge. Since the CarpetDIEM I microphone array is large and perpendicular to the flight path, the potential for carpet width underestimation from the TERRAIN keyword was undesirable.

The F/A-18 F-function input that is built into the PCBoom suite was used at two different starting signature locations, R/L=1 and R/L=10. Results using the F/A-18 F-function input at R/L=1 are located in Appendix B. The F-function input at R/L=10 discussed here is consistent with the R/L used for the CFD input results.

The CFD near-field pressure signatures used in this analysis were provided by Boeing (Shen et al., 2018). The CFD input signatures were generated for the NASA Sonic Booms in Atmospheric Turbulence (SonicBAT) campaign (Bradley et al., 2020), which had similar altitude, Mach number, and weights to the CarpetDIEM I flights. Table 2 gives conditions for two CFD input cases provided by Boeing and compares them with the mean and SD of the trajectory data from CarpetDIEM I for rays that arrived at the ground microphone stations. Case 2 weight was used for the first two passes of each flight at CarpetDIEM I when the aircraft was heavier, while Case 1 weight was used for the last two passes of each flight when the aircraft was lighter due to fuel burn.

Table 2. Conditions used to generate the CFD near-field signatures provided by Boeing compared with CarpetDIEM I aircraft trajectory data.

	Altitude (ft)	**Mach**	**Weight (lbs.)**
CFD conditions	34,000	1.39	Case 1: 29,350 Case 2: 34,050
CarpetDIEM I	Mean: 34,714 SD: 1,427	Mean: 1.31 SD: 0.01	Pass 1: Mean: 33,895, SD: 160 Pass 2: Mean: 32,189, SD: 171 Pass 3: Mean: 30,488, SD: 111 Pass 4: Mean: 28,921, SD: 105

Waveforms produced by near-field inputs are depicted in Figure 2 where the undertrack near-field pressure signatures for the F-function and CFD inputs are at R/L=18, which is the closest distance to the aircraft the waveform can be visualized. The results of the F-function and CFD inputs at R/L=10 are used as input to the Lasso regression in Section IV.

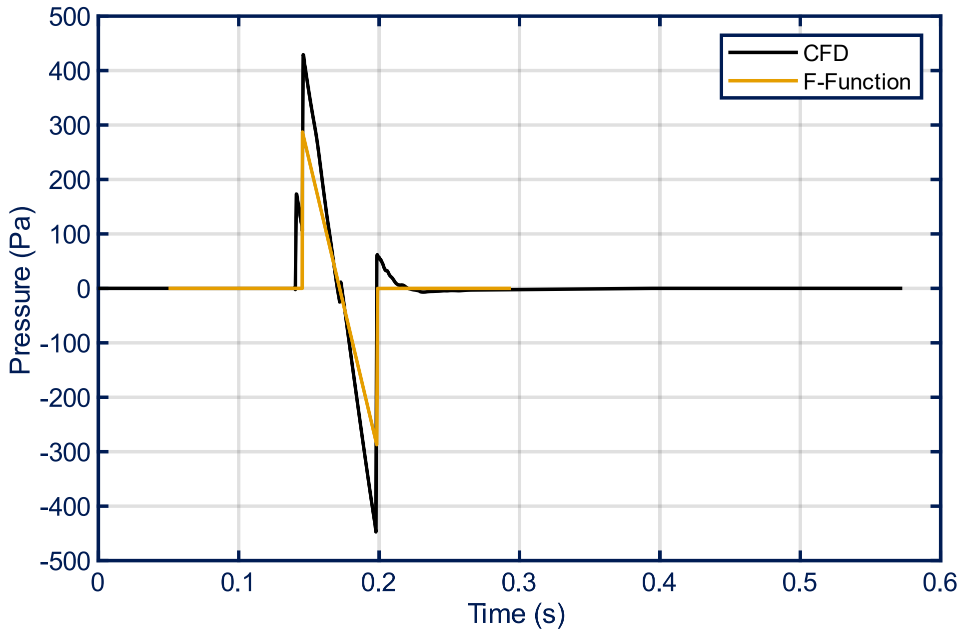

Figure 2. Undertrack near-field pressure signatures for the F/A-18 F-function and CFD inputs at a distance of R/L=18.

B. PCBoom Prediction Accuracy

The propagated predictions are compared to the measurements in this section. First, waveforms for four representative cases are shown. Then differences in peak overpressure and PL between the predictions and measurements are shown. The next subsection includes initial investigations into what may be driving some of the differences between the predictions and measurements.

Predicted (modeled) and measured waveforms that are representative of CarpetDIEM I data are shown in Figure 3. Waveform PL values are noted in the legend, and measurement station locations along the array are illustrated in Figure 3e. Boom 15 at Station 32 (Figure 3a) shows good agreement between the predicted and measured waveforms. Both modeled waveforms slightly underpredict the peak pressure, but the waveform from the CFD input overpredicts while the F-function input underpredicts the level. For the same boom at Station 46 (Figure 3b), the measured waveform shows turbulent spiking with a peak amplitude about 40 Pa greater than either modeled waveform. Again, for the same boom but now at Station 26 (Figure 3c), the peak pressure is greater for the measured waveform than either modeled waveform; however, the F-Function input matches the measured PL within 0.2 dB while the CFD input still overpredicts the PL by 1.7 dB. Lastly, Boom 21 at Station 20 (Figure 3d) demonstrates a case where PCBoom predicted a waveform but the measured data do not show a clean N-wave. Station 26 may have been in or near the shadow zone for Boom 21, which resulted in modeled metrics overpredicting measured PL by about 20 dB.

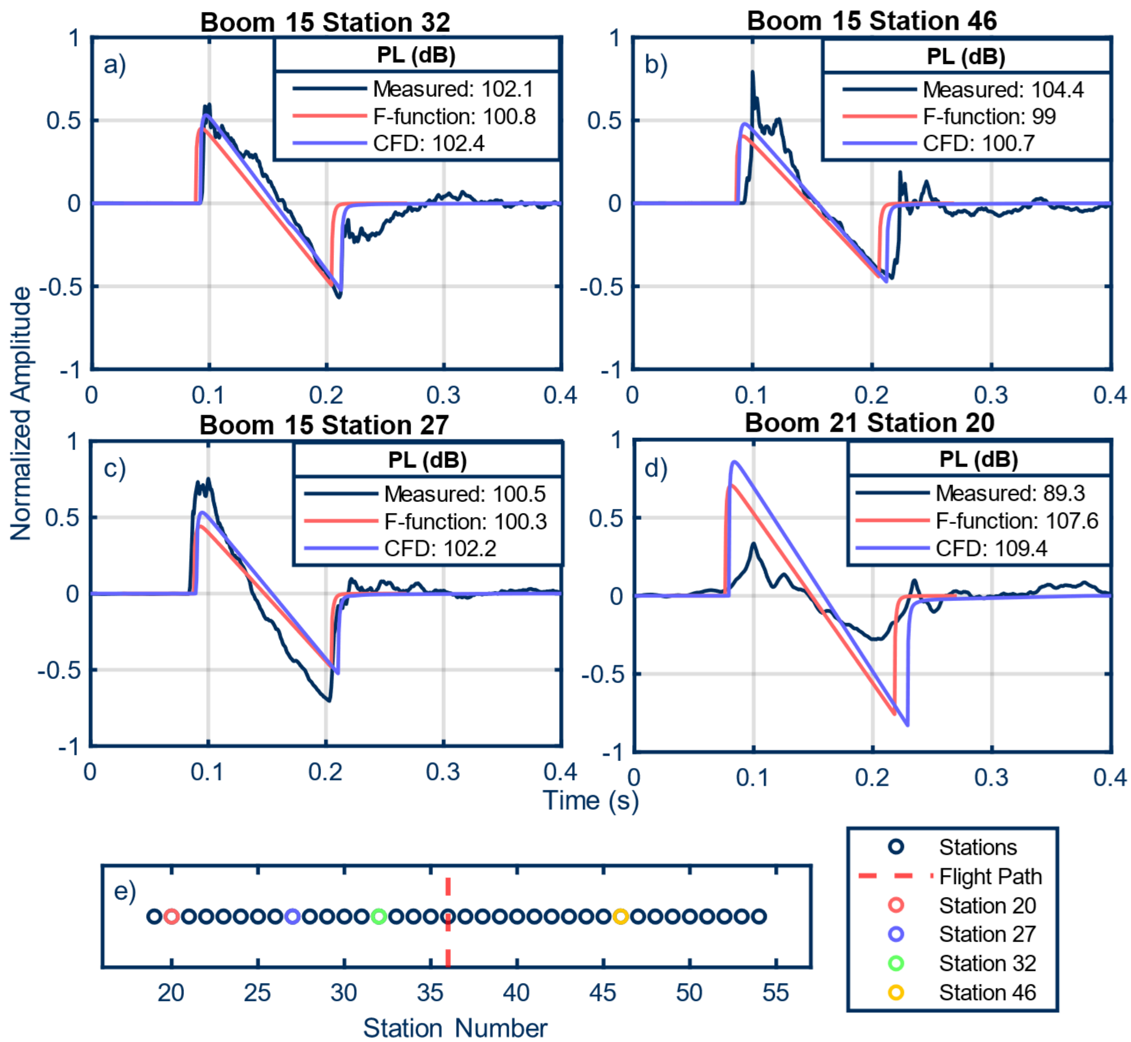

Figure 3. Measured and modeled waveforms for a) Boom 15 at Station 32, b) Boom 15 at Station 46, c) Boom 15 at Station 27, and d) Boom 21 at Station 20 and e) a reference map of station locations relative to the flight path. [Reproduced from Gee et al., (2024)].

Differences in peak pressure between predictions and measurements are shown in Figure 4. On average, PCBoom predictions underestimate the peak pressure for either near-field input. Outliers on the positive end occur when PCBoom predicted a strong N-wave and only a weak waveform or nothing at all was measured. Outliers on the negative end occur when PCBoom predicts weaker waveforms than are measured. Overpredictions were anticipated due to the constant 1.9x ground reflection factor that had been applied to the predicted waveforms regardless of the elevation angle of the ray. This constant ground reflection factor could be inaccurate at higher emission angles where the rays are coming in at close to grazing incidence (Onyeowu, 1975). The underprediction is greater on average for the F-function input at 14.2 Pa than the CFD input at 5.5 Pa. Thus, the predictions from the CFD input are generally more accurate for peak pressure values for the cases studied here.

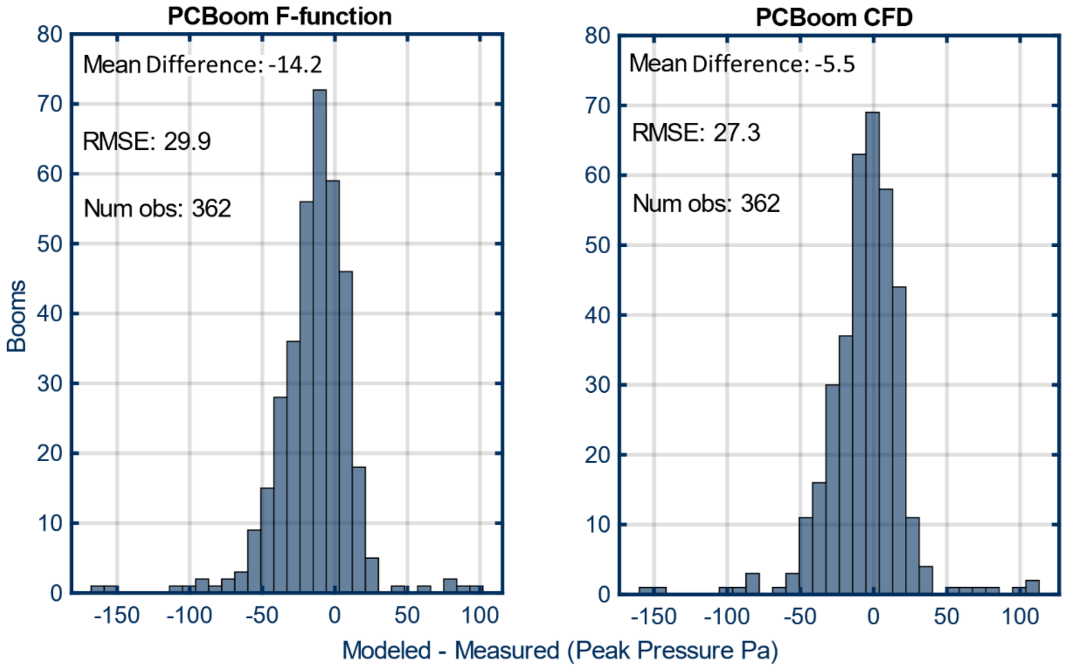

Figure 4. Histogram of differences between PCBoom predictions and measurements for the (left) F-function and (right) CFD near field inputs.

Spectral analysis provides further insight into the discrepancies between the near-field inputs for the modeled predictions and ground-based measurements. Spectral differences are shown in Figure 5 for the mean difference between modeled and measured levels across all booms. The F-function input underpredicts the one-third octave band (OTO) levels below 40 Hz, which are the dominant frequencies for a sonic boom and contribute more to the peak pressure. The F-function input overpredicts OTO levels by up to 8 dB above 40 Hz, which are more heavily weighted in human annoyance metrics such as PL. The CFD input predicts levels rather accurately below 30 Hz but overpredicts levels more than the F-function input does at higher frequencies. These results help explain why the F-function input matched the measured metric levels better than the CFD input despite the waveform mismatch. These results also highlight the inadequacy of either of these quantities (i.e., peak pressures and mean spectral levels) by themselves to fully explain discrepancies between predictions and measurements.

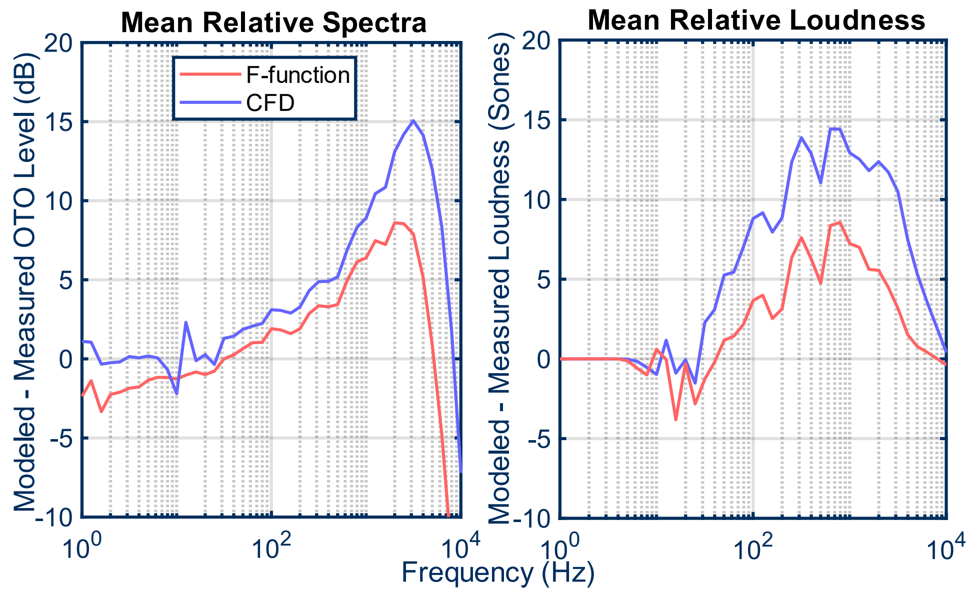

Figure 5. Mean difference between modeled and measured spectral level across all booms in (left) one-third octave band levels and (right) relative loudness in sones.

Differences between predicted and measured metric levels for PL in dB are shown in Figure 6. The mean error bias between modeled and predicted level is positive whereas the mean difference bias for peak pressure in Figure 4 is negative. Interestingly, predictions using the F-function input have a smaller bias and smaller RMSE than predictions using the CFD input. PCBoom with the CFD input overpredicts metrics by an average of 3.2 dB with an RMSE of 5.9 dB, whereas PCBoom with the F-function input overpredicts metrics by an average of 2 dB with an RMSE of 5.3 dB. Results are given in Appendix C for the other five candidate metrics for en-route supersonic aircraft noise certification.

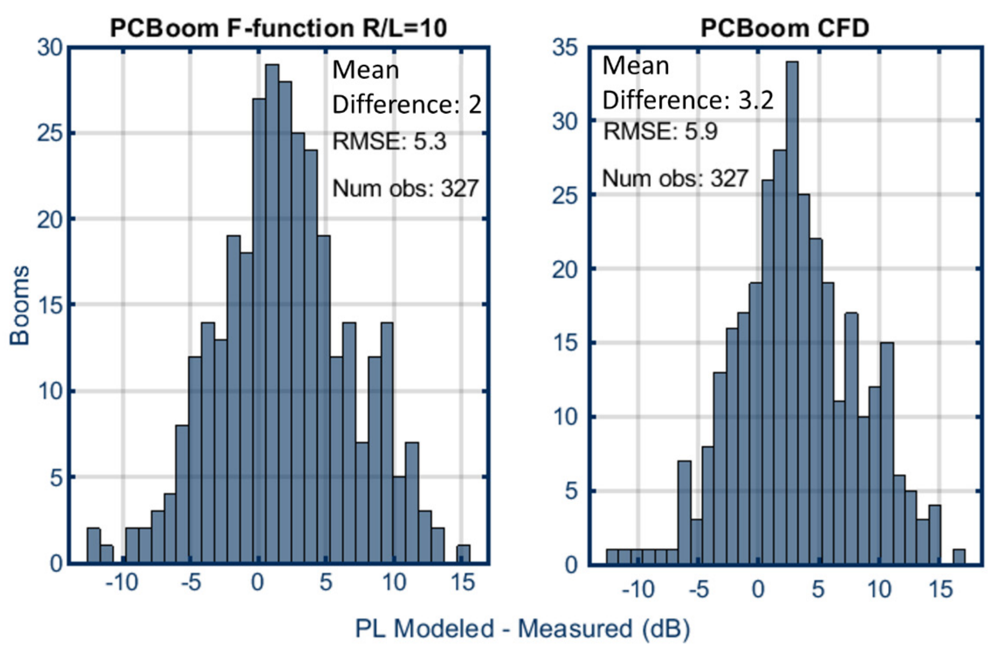

Figure 6. Histograms of level difference between modeled and measured booms for (left) F-function input at R/L=10 and (right) CFD input.

The present analysis differs in approach from the Enhanced Burgers validation work of Lonzaga et al. (2020). Their work used SonicBAT conditions that are closer to those of the Boeing CFD. They showed that the unweighted sound exposure level predictions better matched sailplane measurements (aloft, above the atmospheric boundary layer) when using the CFD solution than the F-function as input. Lonzaga et al. did not show metric levels, which limits potential comparisons between the present work and their study. The difference in measurement location (ground versus above atmospheric boundary layer) also makes direct comparison difficult.

Several limitations of the present analysis of PCBoom may suggest areas of future work. Hardware limitations and ambient noise can distort measurements made on the ground. PCBoom is only as good as its inputs, which include not only near-field pressure but also measured aircraft trajectory data and measured meteorological data from weather balloon launches. Weather balloons at CarpetDIEM I were launched once per flight, and the same data were used for each pass of that flight. Incorporating measurement error from the GPSsonde may be explored in the future as that information is available on its specification sheet (Vaisala, 2018).

Additionally, atmospheric turbulence effects were not considered. Flights occurred in the morning when strong turbulence effects are not expected, and field measurements of turbulence were not made in CarpetDIEM I. It may be possible to estimate turbulence levels with atmospheric model data. Making use of the turbulence modeling modules within PCBoom may improve the prediction results because on average, turbulence reduces the loudness. Turbulence may be an important effect to consider in future work.

In summary, the general trends of the modeling predictions are that the modeled waveforms underpredict the peak pressure and overpredict the loudness. Modeled waveforms generated from the CFD input match the measured waveforms better than the ones generated from the F-function input, but the CFD input overpredict the loudness by a larger amount. On average, PCBoom overpredicts the PL by 2 dB. Examination of spectral differences demonstrated the limitations of using single values like peak pressure or metric levels to quantify prediction accuracy. The following section aims to identify factors that correlate with differences in predictions and measurements.

IV. REGRESSION ANALYSIS

The goal of Section IV is to use Lasso regression to identify factors contributing to metric variability and PCBoom inaccuracies relative to measured data. Data are from CarpetDIEM I, as outlined in Section II, and PCBoom predictions were assessed in Section III. Lasso regression is implemented similar to previous work by Durrant et al. (2022b) as described in Appendix A. In that work, dozens of meteorological, aircraft trajectory, and ambient inputs were narrowed down to a ROM with nine inputs.

A. Lasso Regression Methodology

Lasso regression is an iterative regression technique that can identify and eliminate unimportant predictors from complex datasets (Tibshirani, 1996). Lasso regression is described by Equation 1 as:

$$\text{minimize}\left(\sum_{n=1}^{N}\left(y_n - \sum_{j=1}^{J} x_{nj}\beta_j\right)^2 + \lambda_i \sum_{j=1}^{J} |\beta_j|\right) \quad (1)$$

where the first summation (blue part of the equation) is least squares minimization in multiple dimensions. In this equation, y_n is the output, x_{nj} are the input factors (such as meteorological, aircraft trajectory, or ambient data), and β_j are the regression coefficients of the inputs that obtain the prediction with the lowest squared error. The latter summation (orange part of the equation) is the added Lasso penalty that drives less impactful input coefficients to zero as the penalty factor, λ_i, is increased over each iteration i. The MATLAB `lasso` function (MathWorks, 2022b) was used with 100 iterations, increasing λ until only one or two input coefficients are nonzero by iteration 100. Input parameters are normalized to a mean of 0 and standard deviation of 1.

The next step is to determine the value of λ that produces the best model with Lasso regression. K-fold cross-validation is a common method to determine the λ value (Obuchi and Kabashima, 2016; Chetverikov et al., 2020). At each iteration, data are randomly separated into k subsets, where one subset is used for validation and the rest are used for training. This is repeated k times so that each subset is used once for validation (MathWorks, 2022c). Cross-validation is completed for every iteration, and the λ_i associated with the minimum Mean Squared Error (MSE) is identified. The remaining inputs with nonzero coefficients are identified at this iteration. For a sparser model, the inputs corresponding to one standard error (SE) above the MSE can be used..

An example of 10-fold cross validation is shown in Figure 7. CarpetDIEM I data were used with results over 100 iterations. From left to right, the penalty factor, λ, increases until a minimum MSE is found, as noted by the green circle and vertical dotted line. Several iterations later, the λ value corresponding to one SE above the minimum is indicated by a blue point and dotted line.

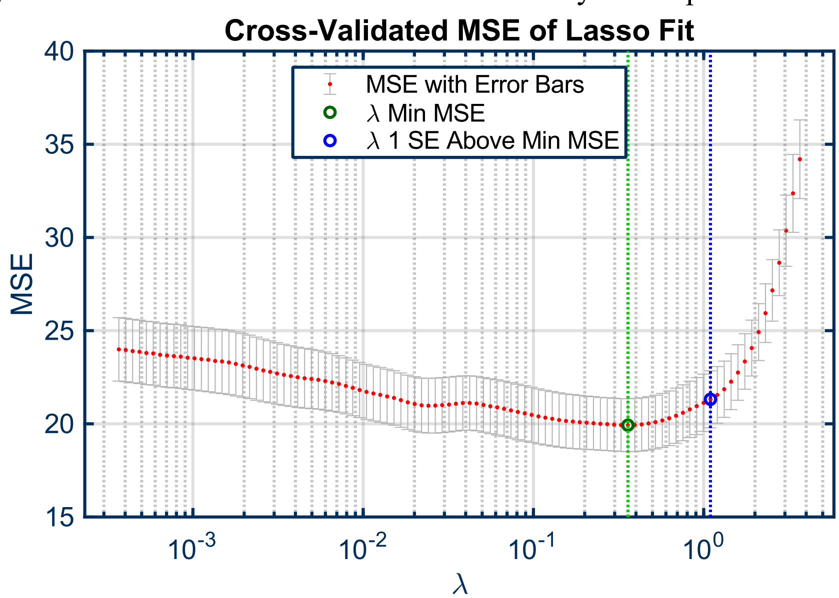

Figure 7. Example Lasso cross-validation results using CarpetDIEM I data. The MSE is given as a function of λ with the minimum noted by a green circle and vertical dotted line and one standard error above the minimum given by the blue circle and vertical dotted line.

This study uses a total of 68 inputs to Lasso regression. These inputs include meteorological data, aircraft trajectory, ambient noise, and PCBoom predictions. Measured meteorological data (e.g., wind speed, temperature, pressure, etc.) were from ground weather stations near the microphone locations and weather balloons launched before each flight to gather atmospheric data for PCBoom. Additionally, modeled turbulence parameters were taken from the Climate Forecast System Version 2 (CFSv2) (Saha et al., 2014). As-flown aircraft trajectory data (e.g., Mach number, heading, flight path angle (FPA), and their derivatives) were also used as input factors. Two sets of ambient noise metrics were calculated, one set for the 650 ms immediately preceding the boom and another set averaged over 60 s before the boom. Finally, PCBoom predictions, including peak pressure and perception metrics, from both F-function and CFD input were used as potential predictors for Lasso. See Appendix D for a full list of Lasso inputs, outputs, and their descriptions.

B. Lasso Results and Analysis

Lasso results are presented in two parts: 1) Lasso predicted noise levels and 2) Lasso predicted noise level differences between measured and modeled data, referred to hereafter as ΔPM.

Lasso results for noise metrics are noted in Table 3. The top 12 factors are listed that minimize the MSE in predicting six measured metrics. Lasso regression is implemented with 10-fold cross validation. The process is replicated 10 times for each of the six metrics because the inputs and outputs for validation are randomized for each iteration and the results are subject to random grouping variation. The maximum “total score” (an ad-hoc measure of predictive power) is 60 for each input as each input could be chosen up to 10 times for six different metrics. The inputs in Table 3 are useful for predicting what was measured at CarpetDIEM I.

Table 3. Lasso results for predicting metrics, arranged by total score. Inputs are listed across the top row and scores for each metric in subsequent rows.

Input:	Straight-line distance	Mach Derivative	Avg. Ambient DSEL	PCBoom F-Function DSEL	Mach 2nd Derivative	Ambient ASEL
PL Score	10	10	10	10	0	10
ASEL Score	10	10	10	9	0	10
BSEL Score	10	10	10	10	10	10
DSEL Score	10	10	10	10	10	0
ESEL Score	10	10	10	10	10	10
ISBAP Score	10	10	10	10	10	0
Total Score	60	60	60	59	40	40

Input:	Flight Path Angle 2nd Derivative	High Alt. Wind Speed	PCBoom F-function Peak Pressure	Ground Wind Direction	Aircraft Heading	Friction Velocity
PL Score	10	0	0	10	2	10
ASEL Score	10	2	0	4	10	3
BSEL Score	10	8	8	0	0	0
DSEL Score	0	10	10	3	0	0
ESEL Score	10	0	0	0	7	0
ISBAP Score	0	10	10	10	0	3
Total Score	40	30	28	27	19	16

Lasso results for the same analysis but for predicting ΔPM are given in Table 4. The top 11 inputs identified in Table 4 agree with many of the same inputs found in Table 3. The inputs in Table 4 are useful for identifying factors that cause differences between PCBoom predictions and measurements.

Table 4. Lasso results for predicting ΔPM, arranged by total score. Inputs are listed across the top row and scores for each metric in subsequent rows.

Input:	Mach Derivative	Mach 2nd Derivative	Flight Path Angle 2nd Derivative	Avg. Ambient DSEL	Straight-line Distance	Heading Derivative
PL Score	10	10	10	10	10	10
ASEL Score	10	10	10	6	10	8
BSEL Score	10	10	10	10	10	1
DSEL Score	10	10	10	10	10	5
ESEL Score	10	10	10	10	10	8
ISBAP Score	10	10	10	10	1	8
Total Score	60	60	60	56	51	40

Input:	Abs. value Emission Angle	Low Alt. Dew Point	High Alt. Pressure	Relative Humidity	Friction Velocity
PL Score	10	10	10	7	5
ASEL Score	1	2	1	5	0
BSEL Score	1	0	0	0	0
DSEL Score	9	0	0	0	0
ESEL Score	0	0	0	0	0
ISBAP Score	10	10	10	1	7
Total Score	31	22	21	13	12

Factors identified in Tables 3 and 4 can be individually investigated to understand how they influence metric variability. Several high-scoring inputs for ΔPM are from aircraft trajectory data, including Mach derivatives, FPA 2nd derivative, and heading derivative. These results are intriguing, as CarpetDIEM I booms were intended to be generated by an F/A-18 aircraft flying at steady conditions with minimal variation from flight to flight.

Aircraft trajectory variation on PCBoom predictions are shown in Figure 8. Three Lasso-identified aircraft trajectory inputs are plotted against ΔPM in PL, or ΔPM_{PL}. Points are colored by station number to identify off-track distance. Similar trends are found for the three different inputs. On average, ΔPM_{PL} increases with Mach derivatives. Conversely, ΔPM_{PL} decreases as FPA 2nd derivative increases. Many of the largest outliers correspond to steady flight (i.e., derivatives of Mach and FPA are close to zero) and at far off-track ground microphone stations (yellow and dark blue circles). Furthermore, many stations near the middle of the array (stations 30 to 40 with colors light blue to green) have nonzero Mach derivatives and FPA values, indicating non-steady flight on closer approach to the array.

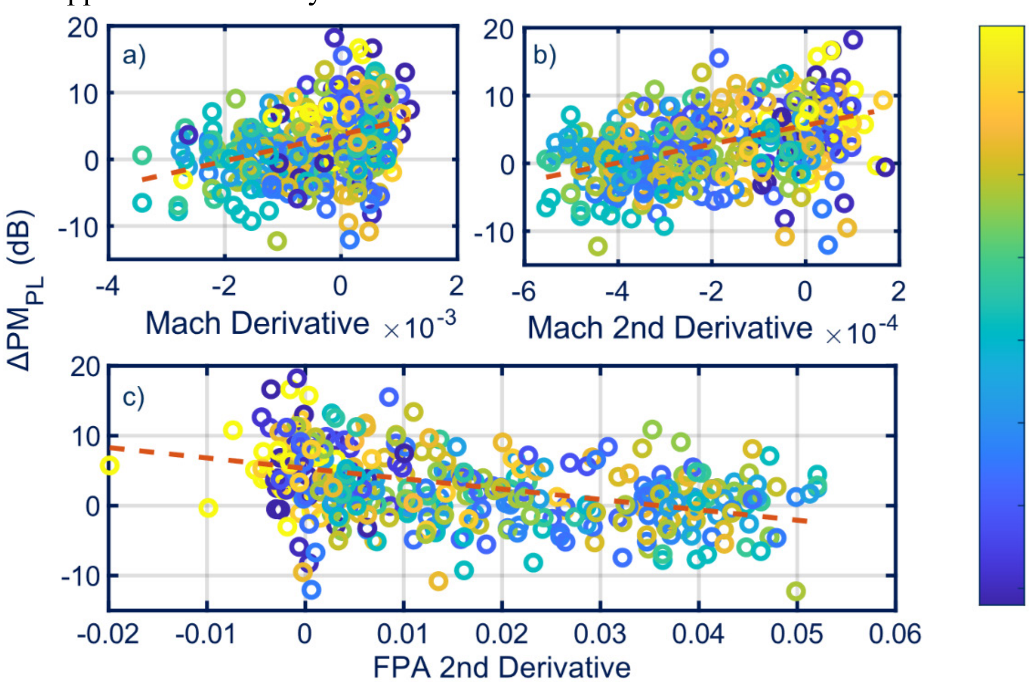

Figure 8. Aircraft trajectory data versus ΔPM_{PL} for a) Mach Derivative, b) Mach 2nd Derivative, and c) Flight Path Angle (FPA) 2nd Derivative.

Example aircraft trajectories are visualized in Figure 9 and Figure 10. Top-down views are shown of the PCBoom-predicted ray landing positions (gray dots), as-flown flight trajectories (colored by Mach number), ground measurement stations (red and green circles), and the emission ray (blue dashed lines) that connect the boom propagation path from the aircraft to the measurement array. A relatively steady flight (Flight 2 Pass 2) with a boom carpet that covers all ground stations is shown in Figure 9. An additional flight (Flight 5 Pass 2) is shown in Figure 10 with greater deceleration, a different heading, and sharper turn near the array that results in a carpet that barely covers the southernmost stations.

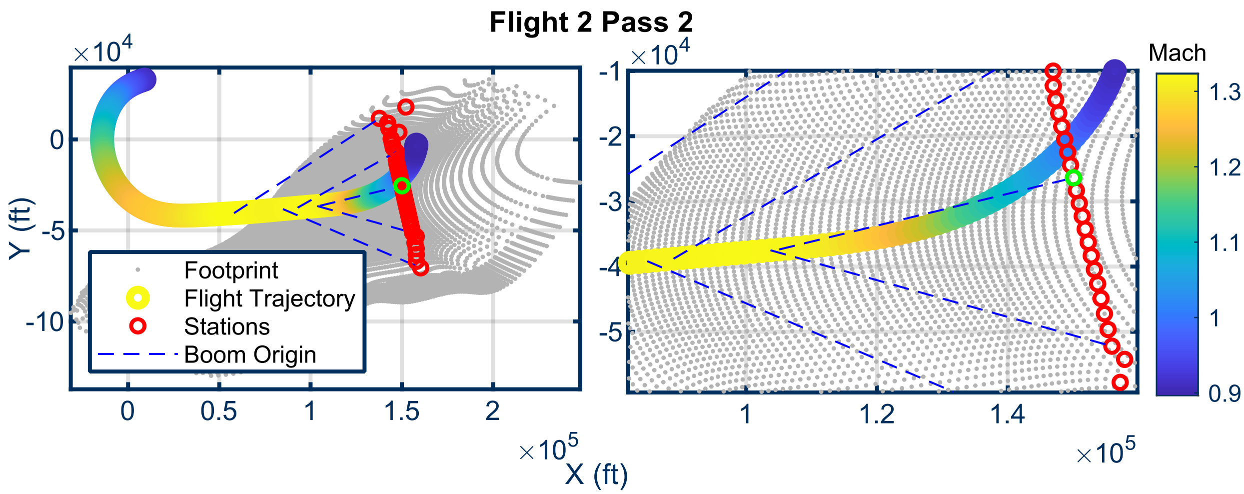

Figure 9. (Left) PCBoom footprints (gray dots) with as-flown flight trajectories (colored by Mach number), ground measurement sites 19 to 54 (red circles), and emission rays (blue dashed lines) for Flight 2 Pass 2. (Right) A zoomed-in view of the same pass.

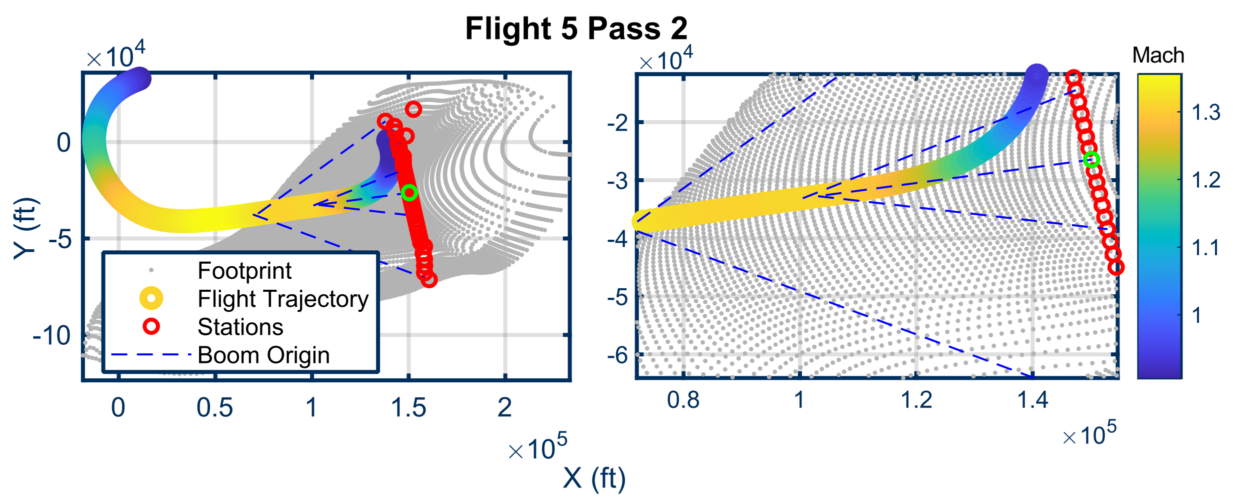

Figure 10. (Left) PCBoom footprints (gray dots) with as-flown flight trajectories (colored by Mach number), ground measurement sites 19 to 54 (red circles), and emission rays (blue dashed lines) for Flight 5 Pass 2. (Right) A zoomed-in view of the same pass.

Comparing these two supersonic passes provides insight into the impact of aircraft trajectory factors. Most emission rays were emitted when the aircraft trajectory was steady and level. However, in several passes, such as the one shown in Figure 10, the aircraft emitted the undertrack rays as it started to decelerate and turn. The measurement stations at the center of the array are more likely to receive rays that correspond to a changing trajectory. This could explain why Lasso identified aircraft trajectory factors as influencing metrics: the derivatives are changing at the same time the loudest rays are emitted. These results suggest that future testing with the X-59 aircraft should extend the steady, level flight track to ensure the entire array measures supersonic noise signatures from steady cruise conditions.[3]

Some factors from the Lasso regression results for ΔPM in Table 4 suggest PCBoom predictions are more accurate undertrack. Figure 11 and Figure 12 plot the straight-line distance and absolute values of the emission ray angle against ΔPM_{PL} with a linear fit and confidence bounds. Larger straight-line distance and absolute values of the emission ray angle correspond with off-track distance. Both factors have a positive trend with ΔPM_{PL} and trend towards zero for undertrack rays (where emission angle approaches zero and straight-line distances is at its minimum of about 51,000 ft). These results suggest PCBoom is more accurate at undertrack predictions than at off-track locations.

A couple of hypotheses are considered for the factors contributing to the larger ΔPM_{PL} at off-track locations. One possible reason could be the use of a constant ground reflection factor. This factor may be less accurate for grazing incidences at off-track sites. Another possible explanation could be the farther propagation of off-track rays through more of the atmospheric boundary layer. Turbulence in the atmospheric boundary layer can cause a mean reduction in loudness in addition to random spiking and flattening of the waveforms (Lonzaga, 2021).

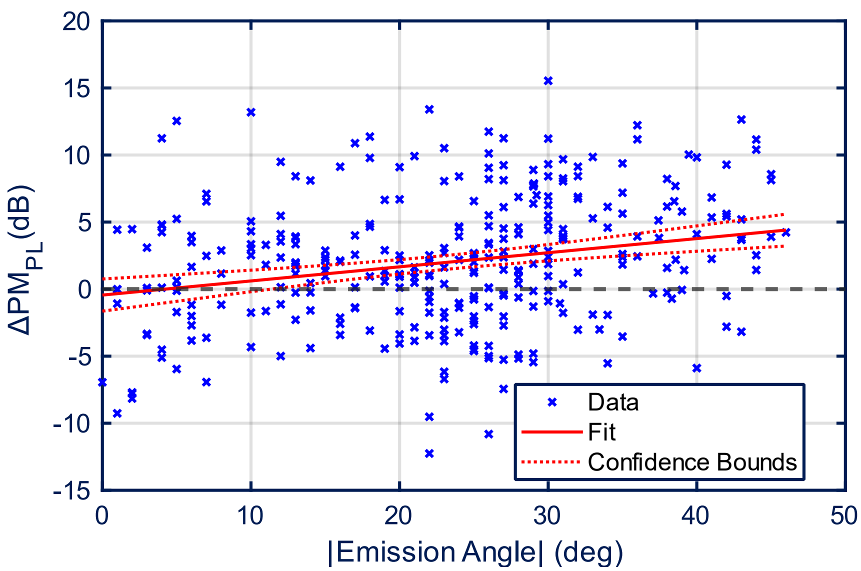

Figure 11. Absolute value of emission angle versus ΔPM_{PL} with a linear fit and confidence bounds.

[3] In conversation with CarpetDIEM I principal investigators, they revealed that the steady cruise portion of the flight track was intentionally short for CarpetDIEM I in order to get as many passes as possible. This will not be the case for Quesst Phase 2 as flight tracks will not be shortened.

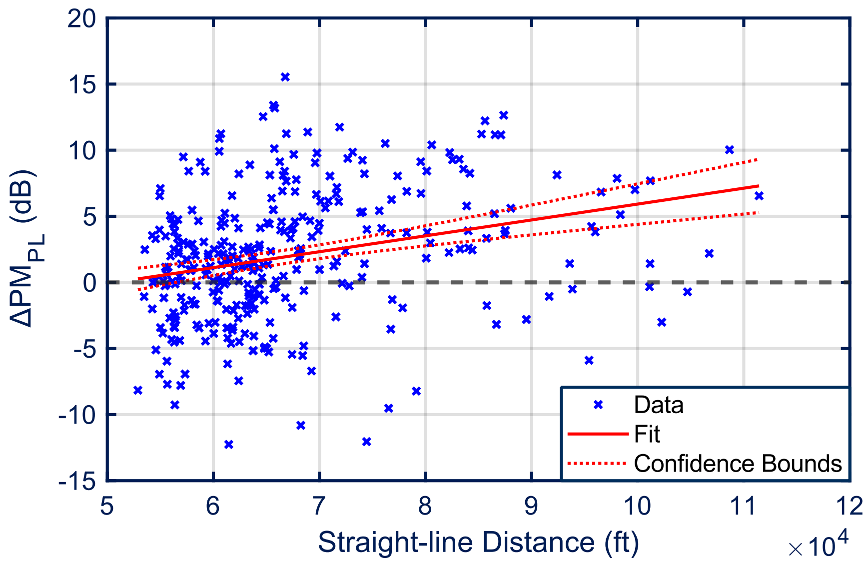

Figure 12. Straight-line distances versus ΔPM_{PL} with a linear fit and confidence bounds.

In this section, Lasso regression identified several contributors to metric variability and PCBoom inaccuracy at CarpetDIEM I. The identification of several unexpected parameters related to the flight trajectory guided a deeper investigation into factors and why they may be contributing to the variability and metric misestimations. These factors can be incorporated into a ROM for both predicting metrics and ΔPM.

C. Reduced-Order Model Implementation

A ROM can be developed from the Lasso-identified inputs that contribute most to the metric variability and PCBoom inaccuracy. Lasso regression narrowed down the 68 inputs to 12 and 11 inputs for predicting metrics and ΔPM, respectively. A ROM can include all of these inputs or just a few to predict metrics or aid PCBoom predictions. This section investigates using all 12 and 11 inputs to develop ROMs.

The predictive capabilities of a ROM are assessed using LSQ regression. Table 5 shows the results of LSQ regression on the 12 inputs obtained from Lasso regression to predict PL. Large p-values for many of the inputs indicate important factors and may suggest that a sparser model could be implemented. Inputs are mean-centered and scaled by standard deviation to assess the relative weight of each input. The impact on PL can be directly assessed by comparing coefficient magnitudes. The inputs with the greatest impact on PL are straight-line distance and PCBoom F-function peak pressure, followed by Mach derivative.

Some physical rationale can be inferred from the positive or negative coefficient trends. The positive coefficients for ambient noise inputs may suggest that either ambient noise causes an increase in metric values or it is the best predictor outside the boom carpet where only ambient noise was recorded. Negative coefficients indicate an inverse relationship between the input and PL. The friction velocity is negative, implying that increasing turbulence reduces the noise level, which is well-established in the literature (Lonzaga, 2022b).

Table 5. Coefficients and p-values from LSQ regression for predicting PL.

Input:	Straight-line Distance	Mach Derivative	Avg. Ambient DSEL	PCBoom F-function DSEL	Mach 2nd Derivative	Ambient ASEL
Coefficient:	-1.8	-0.8	0.7	0.7	0.1	0.03
p-value:	0.08	0.06	0.4	0.7	0.9	0.97

Input:	Flight Path Angle 2nd Derivative	High Alt. Wind Speed	PCBoom F-function Peak Pressure	Ground Wind Direction	Aircraft Heading	Friction Velocity
Coefficient:	0.65	0.07	1.3	-0.3	-0.09	-0.2
p-value:	0.3	0.8	0.5	0.4	0.8	0.5

Predictions from the ROM and PCBoom F-function are now compared. Distributions of prediction errors in Figure 13 are given as the difference between the modeled predictions from the ROM or PCBoom and the measured data. The RMSE for the ROM is 4.5 dB while the RMSE for ΔPM_{PL} from PCBoom is 5.3 dB. Furthermore, the SD of the measured PL values is 7.4 dB (see Table 1). The analysis shows that supplementing PCBoom predictions with other parameters can improve the prediction of PL. This comparison does not suggest replacing PCBoom with a ROM but instead shows how much variability in boom metric predictions can be accounted for by these 12 inputs.

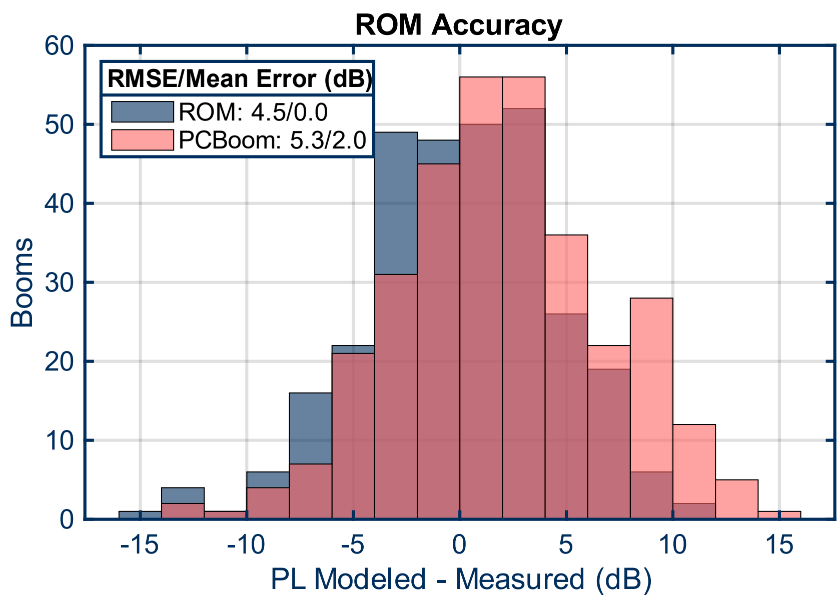

Figure 13. Distributions of prediction error comparing the ROM and the PCBoom F-function predictions relative to measured PL values.

In addition to predicting metrics, the ROM can be used to aid PCBoom predictions. Results are given in Table 6 for the 11-inputs included in the ROM for predicting ΔPM_{PL}. Several meteorological inputs, such as humidity and high-altitude pressure, have low p-values. Straight-line distance and heading derivative have the lowest p-values. These results identify inputs that are contributing the most to the mismatch between predictions and measurements.

Table 6. Coefficients and p-values from LSQ regression for predicting ΔPM_{PL}.

Input:	**Mach Derivative**	**Mach 2nd Derivative**	**Flight Path Angle 2nd Derivative**	**Avg. Ambient DSEL**	**Straight-line Distance**	**Heading Derivative**
Coefficient:	0.2	-0.4	-1.3	-0.6	1.8	2.1
p-value:	0.6	0.6	0.05	0.05	0.01	< 0.001

Input:	**Abs. value Emission Angle**	**High Alt. Pressure**	**Low Alt. Dew Point**	**Relative Humidity**	**Friction Velocity**
Coefficient:	-0.4	-1.5	-0.5	-1.0	-0.2
p-value:	0.45	0.03	0.4	0.03	0.7

The ROM-aided PCBoom predictions are compared with regular PCBoom predictions in Figure 14. The ΔPM_{PL} histogram (red) has a larger RMSE and mean error than the ROM-aided ΔPM_{PL} histogram (blue). The ROM is able to reduce the RMSE of PCBoom by 0.6 dB and reduce the mean error from 2 dB to -0.4 dB.

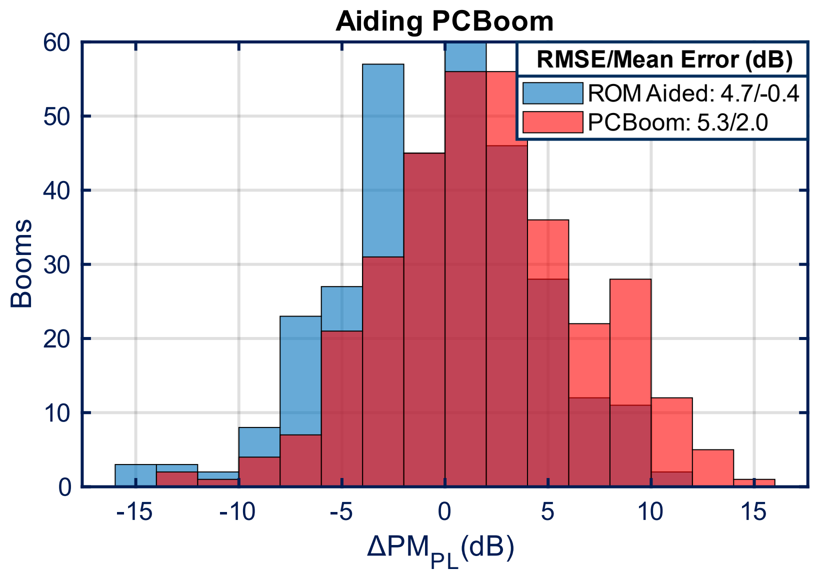

Figure 14. Distributions of prediction error comparing the PCBoom predictions aided by ROM and the PCBoom predictions without ROM assistance relative to measured PL values.

The results of the ROM are effective for the present dataset but may be limited in application to other datasets. The intent of this work is to establish a framework for the Lasso and LSQ regression analyses that can be used for future studies. Data from multiple studies would be more ideal for developing a ROM that has most extensive applicability. But rather than focusing on ROM development, results from this study can be used to guide efforts to further investigate areas for PCBoom improvement.

D. Limitations

Two key limitations of the Lasso parameter selection process are noted here. First, the input parameters to Lasso regression are highly correlated. Table 7 notes the correlation values for the 12 inputs used for metric prediction (see Table 5), and Table 8 notes the correlation values for the 11 inputs used for ΔPM_{PL} prediction (see Table 6). For the correlation values of all 68 inputs, see Appendix E. Some inputs, like straight-line distance and horizontal distance, are nearly perfectly correlated with a correlation value of 0.999. Highly correlated inputs can be used interchangeably in a ROM with similar performance. Also, some eliminated inputs from the model may be highly correlated to those within the model. Thus, it is helpful to not just use the top factors but to also consider their correlates.

Second, the identified inputs and developed ROM might not be generalizable to other datasets. Lasso did identify several of the same parameters for both CarpetDIEM and QSF18 (see Appendix A). However, it is unknown whether these same parameters will be applicable to a quiet supersonic noise signature produced by the X-59 aircraft. Furthermore, results could change if turbulence effects are accounted for in the modeled waveforms. Therefore, the applicability of the developed ROM may be limited to the current dataset.

Table 7. Top correlations for inputs that predict PL. Note: this table's format mirrors Table 5.

Input:	**Straight-line distance**	**Mach Derivative**	**Avg. Ambient DSEL**	**PCBoom F-Function DSEL**	**Mach 2nd Derivative**	**Ambient ASEL**
1	Horizontal Distance 0.999	Mach 2nd Derivative 0.713	Avg. Ambient ESEL 0.994	PCBoom F-Function ESEL 0.999	Straight-line Distance 0.764	Ambient PL 0.998
2	Emission Angle Squared 0.796	Abs. Value Emission Angle 0.525	Avg. Ambient PL 0.991	PCBoom F-Function BSEL 0.997	Horizontal Distance 0.751	Ambient ESEL 0.993
3	Mach 2nd Derivative 0.764	Emission Angle Squared 0.481	Avg. Ambient ASEL 0.989	PCBoom F-Function ASEL 0.997	Mach Derivative 0.713	Ambient DSEL 0.967
4	Abs. Value Emission Angle 0.757	Straight-line distance 0.470	Avg. Ambient ISBAP 0.981	PCBoom F-Function ISBAP 0.993	Emission Angle Squared 0.594	Avg. Ambient ESEL 0.943
5	Mach Derivative 0.470	Horizontal Distance 0.465	Avg. Ambient BSEL 0.954	PCBoom F-Function PL 0.990	Abs. Value Emission Angle 0.571	Avg. Ambient ASEL 0.942

Input:	Flight Path Angle 2nd Derivative	High Alt. Wind Speed	PCBoom F-function Peak Pressure	Ground Wind Direction	Aircraft Heading	Friction Velocity
1	Flight Path Angle 1st Derivative 0.916	Low Alt. Humidity 0.789	PCBoom BSEL 0.981	Atmospheric Boundary Layer Height 0.516	X-Plane 0.977	Mark time 0.747
2	FPA 0.408	Low Dew 0.743	PCBoom DSEL 0.980	High Temp 0.496	Y-Plane 0.956	High Alt. Wind Direction 0.676
3	Low Alt. Wind Speed 0.407	Friction Velocity 0.486	PCBoom Peak Pressure 0.979	Low Alt. Pressure 0.487	Altitude 0.688	Temperature 0.668
4	High Alt. Temperature 0.403	High Alt. Wind Direction 0.391	PCBoom ESEL 0.978	Mark Time 0.468	Flight Number 0.477	Atmospheric Boundary Layer Height 0.641
5	Low Alt. Pressure 0.335	Altitude 0.311	PCBoom ASEL 0.968	Low Alt. Wind Speed 0.420	Pass Number 0.448	High Alt. Wind Speed 0.486

Table 8. Top correlations for inputs that predict ΔPM_{PL}. Note: this table's format mirrors Table 6.

Input:	**Mach Derivative**	**Mach 2^{nd} Derivative**	**Flight Path Angle 2^{nd} Derivative**	**Avg. Ambient DSEL**	**Straight-line Distance**	**Heading Derivative**
1	Mach 2^{nd} Derivative 0.713	Straight-line Distance 0.764	Flight Path Angle 1^{st} Derivative 0.916	Avg Ambient ESEL 0.994	Horizontal Distance 0.999	Abs. Value Emission Angle 0.383
2	Abs. Value Emission Angle 0.525	Horizontal Distance 0.751	Flight Path Angle 0.408	Avg. Ambient PL 0.991	Emission Angle Squared 0.796	Emission Angle Squared 0.348
3	Emission Angle Squared 0.481	Mach Derivative 0.713	Low Alt. Wind Speed 0.407	Avg Ambient ASEL 0.989	Mach 2^{nd} Derivative 0.764	PCBoom Distance 0.339
4	Straight-line Distance 0.470	Emission Angle Squared 0.594	High Alt. Temp 0.403	Avg Ambient ISBAP 0.981	Abs. Value Emission Angle 0.757	Straight-line Distance 0.330
5	Horizontal Distance 0.465	Abs. Value Emission Angle 0.571	Low Alt. Pressure 0.335	Avg Ambient BSEL 0.954	Mach Derivative 0.470	Horizontal Distance 0.330

Input:	Abs. value Emission Angle	High Alt. Pressure	Low Alt. Dew Point	Relative Humidity	Friction Velocity
1	Emission Angle Squared 0.962	Low Alt. Pressure 0.837	Low Alt. Relative Humidity 0.964	Low Alt. Wind Direction 0.501	Mark Time 0.747
2	Horizontal Distance 0.776	Low Alt. Wind Speed 0.779	High Alt. Wind Speed 0.743	Low Alt. Relative Humidity 0.426	High Alt. Wind Direction 0.676
3	Straight-line Distance 0.757	Low Alt. Temperature 0.737	Low Alt. Wind Direction 0.670	Low Alt. Dew Point 0.282	Temperature 0.668
4	Mach 2nd Derivative 0.571	High Alt. Temperature 0.615	High Alt. Wind Direction 0.504	High Alt. Wind Speed 0.187	Atmospheric Boundary Layer Height 0.641
5	Mach Derivative 0.525	High Alt. Dew Point 0.570	Friction Velocity 0.289	Mach 2nd Derivative 0.184	High Alt. Wind Speed 0.486

V. CONCLUDING REMARKS

This work demonstrated Lasso regression on sonic boom data to identify contributors to measurement variability and prediction misestimation. Measurement data were from NASA CarpetDIEM I flight test campaign with an F/A-18 A aircraft. Predictions were modeled using PCBoom version 7.2 with Enhanced Burgers module with two near-field input types: F-function and CFD. The measured data were compared with the modeled predictions and then further investigated with Lasso regression.

For the CarpetDIEM I dataset, the F-function near-field input produced a better match to the measured metrics than the CFD input. In general, modeled waveforms underpredicted peak pressure and overpredicted the loudness. The CFD input matched measured waveforms better but overpredicted loudness by a larger amount than the F-function input. On average, the models overpredicted PL by 2 dB, which is attributed to high frequency content that is weighted more in the metric calculations. Notably, turbulence effects may be relevant but are not accounted for in this analysis.

Lasso regression identified several contributors to metric variability and PCBoom inaccuracy at CarpetDIEM I. From 68 inputs, a subset of 11 or 12 inputs were identified as top contributors, several of which are highly correlated with others. Further investigating the identified trajectory-related factors revealed that the steady, level portion of the flight tracks were shorter than anticipated.

From the top Lasso-identified factors, a ROM can be developed to predict metrics. The ROM in this study improved metric prediction by lowering the RMSE by 0.6 dB and centering the mean error closer to zero. Potentially, fewer inputs could be used to create an even simpler ROM with similar predictive capabilities. A ROM could be used to aid PCBoom predictions; however, the ROM developed in this study might not be readily applicable beyond the CarpetDIEM I dataset. The regression analyses demonstrated in this work provide a framework for future studies to further investigate and improve predictions of sonic booms.

References

Anderson, M. C., Gee, K. L., Durrant, J. T., Loubeau, A., Doebler, W. J., and Klos, J. (**2024**). "Reducing contaminating noise effects when calculating low-boom loudness levels," J. Acoust. Soc. Am. 155(6), 3889–3899. https://doi.org/10.1121/10.0026436

Baudoin, M., Coulouvrat, F., and Thomas, J. (**2011**). "Sound, infrasound, and sonic boom absorption by atmospheric clouds," J. Acoust. Soc. Am. 130, 1142–1153. https://doi.org/10.1121/1.3619789

Bradley, K. A., et al. (**2020**). "Sonic Booms in Atmospheric Turbulence (SonicBAT): The Influence of Turbulence on Shaped Sonic Booms," NASA/CR-2020-220509, NASA Armstrong Flight Research Center, Edwards, CA. https://ntrs.nasa.gov/citations/20200002482

Carlson, H. W., Mack, R. J., and Morris, O. A. (**1966**). "Sonic Boom Pressure-Field Estimation Techniques," J. Acoust. Soc. Am. 39(5), S10–S18. https://doi.org/10.1121/1.1914038

Chetverikov, D., Liao, Z., and Chernozhukov, V. (**2021**). "On cross-validated Lasso in high dimensions," Ann. Statist. 49, 1300–1317. https://doi.org/10.1214/20-AOS200

Downs, R., Page, J. A., Durrant, J. T., Gee, K. L., Novakovich, D. J., Anderson, M. C., and Loubeau, A. (**2022**). "Sonic boom measurements: Practical implications considering ground effects, microphone installation, and weather hardening." JASA Express Lett. 2, 104001. https://doi.org/10.1121/10.0014414

Durrant, J. T., Gee, K. L., Anderson, M. C., Cook, M. R., and Loubeau, A. (**2021**). "Preliminary lasso regression analysis of environmental effects on sonic boom metric variability [Conference Presentation]," J. Acoust. Soc. Am. 150, A259. Conference presentation abstract: https://doi.org/10.1121/10.0008215.

Durrant, J. T., Gee, K. L., Anderson, M. C., Mathews, L. T., Rasband, R. D., Novakovich, D. J., Loubeau, A., and Doebler, W. J. (**2022a**). "An overview of Brigham Young University's participation in NASA's CarpetDIEM campaign," Proc. Mtgs. Acoust. 43, 045002. https://doi.org/10.1121/2.0001589

Durrant, J. T., Gee, K. L., Anderson, M. C., Cook, M. R., Loubeau, A., and Doebler, W. J. (**2022b**). "Regression analysis of meteorological, aircraft trajectory, and ambient effects on sonic boom metric variability [Conference Presentation]," J. Acoust. Soc. Am. 151, A87. Conference presentation abstract: https://doi.org/10.1121/10.0010745

Durrant, J. T., Anderson, M. C., Gee, K. L., Mathews, L. T., and Hart, G. W. (**2022c**). "Initial comparison of a Falcon-9 reentry sonic boom with other launch-related noise," Proc. Mtgs. Acoust. 46, 045002. https://doi.org/10.1121/2.0001579

Gee, K. L., Anderson, M. C., Nyborg, K. Durrant, J. T., Blaine, J. D., Sorrell, A. K. (**2024**). "Sonic Boom Analyses in Support of Improved X-59 Community Noise Testing," NASA/CR-20240008985, NASA Langley Research Center, Hampton, VA. https://ntrs.nasa.gov/citations/20240008985

Haering, E. A. J. W. Smolka, Murray, J. E., and Plotkin, K. J. (**2006**). "Flight Demonstration Of Low Overpressure N-Wave Sonic Booms and Evanescent Waves," AIP Conf. Proc. 838, 647-650. https://doi.org/10.1063/1.2210436.

Lonzaga, J. B., (**2019**). “Recent Enhancements to NASA’s PCBoom Sonic Boom Propagation Code,” in AIAA Aviation 2019 Forum, Dallas, TX. https://doi.org/10.2514/6.2019-3386

Lonzaga, J. B., Doebler, W. J., Loubeau, A., Aumann, A., Page, J. A., and Shumway, M. (**2020a**). “Latest Release of Fast PCBoom Code for Sonic Boom Propagation [Conference Presentation],” NASA Acoustics Technical Working Group Meeting, NASA Langley Research Center, Hampton, VA. Presentation slides: https://ntrs.nasa.gov/citations/20205009119

Lonzaga, J. B. (**2020b**). “Advanced sonic boom propagation model based on a single-ray Jacobian [Conference Presentation],” J. Acoust. Soc. Am. 148, 2524. Conference presentation abstract: https://doi.org/10.1121/1.5147011

Lonzaga, J. B. (**2021**). “Distortion and losses of sonic booms through turbulent fields [Conference Presentation],” J. Acoust. Soc. Am. 149, A74. Conference presentation abstract: https://doi.org/10.1121/10.0004558; Presentation slides: https://ntrs.nasa.gov/citations/20210015045.

Lonzaga, J. B. et al. (**2022a**). “PCBoom Version 7 Technical Reference", NASA/TM-20220007177, NASA Langley Research Center, Hampton, VA (2022). https://ntrs.nasa.gov/citations/20220007177

Lonzaga, J. B. (**2022b**). "A spatial averaging of sonic boom waveforms [Conference Presentation]," J. Acoust. Soc. Am. 151, A86. Conference presentation abstract: https://doi.org/10.1121/10.0010742

MathWorks (**2022a**). *fitlm*, https://www.mathworks.com/help/stats/fitlm.html, accessed June 9, 2022.

MathWorks (**2022b**). *lasso*, https://www.mathworks.com/help/stats/lasso.html , accessed August 2, 2022.

MathWorks (**2022c**). *Cross-Validation,* https://www.mathworks.com/discovery/cross-validation.html, accessed August 4, 2022.

Obuchi, T. and Kabashima, Y. (**2016**). “Cross validation in LASSO and its acceleration,” J. Stat. Mech., 053304. https://doi.org/10.1088/1742-5468/2016/05/053304

Onyeowu, R. O. (**1975**). “Diffraction of Sonic Boom Past the Nominal Edge of the Corridor,” J. Acoust. Soc. Am. 58(2), 326–330. https://doi.org/10.1121/1.380676

Page, J. A., Plotkin, K. J., and Wilmer, C. (**2010**). “PCBoom Version 6.6 Technical Reference and User Manual,” Tech. Rep., WYLE LABORATORIES, INC.

Page, J. A. and Loubeau, A. (**2019**). “Overall vehicle system noise: sonic boom,” CEAS Aeronaut. J. 10, 335–353. https://doi.org/10.1007/s13272-019-00379-0

Page, J. A., et al. (**2020a**). “Quiet Supersonic Flights 2018 (QSF18) Test: Galveston, Texas Risk Reduction for Future Community Testing with a Low-Boom Flight Demonstration Vehicle (Volume 1),” NASA/CR-2020-220589/Volume I. https://ntrs.nasa.gov/citations/20200003223

Page, J. A., et al. (**2020b**). “Quiet Supersonic Flights 2018 (QSF18) Test: Galveston, Texas Risk Reduction for Future Community Testing with a Low-Boom Flight Demonstration Vehicle

(Volume 2)," NASA/CR-2020-220589/Appendices/Volume II. https://ntrs.nasa.gov/citations/20200003224

Page, J. A., et al. (**2020c**). "PCBoom Version 7.1 User's Guide," NASA/TM-20205007703, NASA Langley Research Center, Hampton, VA. https://ntrs.nasa.gov/citations/20205007703

Rathsam, J., Coen, P., Loubeau, A., Ozoroski, L. and Shaw, G. (**2023**). "Scope and goals of NASA's Quesst Community Test Campaign with the X-59 aircraft," in 14th ICBEN Congress on Noise as a Public Health Problem, Belgrade, Serbia. https://icben2023.com/download-paper/presenting63.pdf

Saha, S., et al. (**2014**). "The NCEP climate forecast system," J. Clim. 27, 2185–2208. https://doi.org/10.1175/JCLI-D-12-00823.1

Shen, H., Ladd, J., and Michal, T. (**2018**). "F/A-18B Sonic Boom Near-Field CFD for FAA - in support of SSTG procedures subgroup efforts," ICAO, CAEP WG1 Meeting, September 5, 2018.

Stevens, S. S. (**1972**). "Perceived level of noise by Mark VII and decibels (E)," J. Acoust. Soc. Am. 51(2B), 575–601. https://doi.org/10.1121/1.1912880.

Tibshirani, R. (**1996**). "Regression Shrinkage and Selection via the Lasso," J. R. Stat. Soc. Ser. B Stat. Method. 58, 267–288. https://doi.org/10.1111/j.2517-6161.1996.tb02080.x

Vaisala Oyj (**2018**). "User Guide: Vaisala Radiosonde RS41-SG and RS41-SGP," M211667EN-G, Vantaa, Finland, (**2018**); https://docs.vaisala.com/r/M211667EN-H/en-US

Wang, Y., Zou, Y., Henrickson, K., Wang, Y., Tang, J., and Park, B. J. (**2017**). "Google Earth elevation data extraction and accuracy assessment for transportation applications," PloS One 12, e0175756. https://doi.org/10.1371/journal.pone.0175756

Acknowledgments
Thank you to the NASA Commercial Supersonic Technology team for making this analysis possible. Thank you to Mylan Cook and Mark Transtrum from BYU, who provided valuable feedback on the Lasso and LSQ regression methods. Thank you to Hao Shen for the Boeing F/A-18 CFD data. And finally, a special thank you to Mark Anderson, who helped with code development, troubleshooting, and general support on this project.

Appendix A: Regression analysis of sonic boom data from Quiet Supersonic Flights 2018

NASA conducted the Quiet Supersonic Flights 2018 (QSF18) test in preparation for future community testing with the X-59 aircraft (Page et al., 2020a; Page et al., 2020b). The QSF18 campaign was conducted in Galveston, Texas in the fall of 2018. An F/A-18 A performed low-boom dive maneuvers to produce low-amplitude sonic booms (Hearing et al., 2006). Annoyance responses were collected via survey from the Galveston community.

To produce a dose-response relationship, noise dose values were computed for each sonic boom from a combination of modeled predictions and measured metric values. The physics-based predictions were modeled using PCBoom version 6.7 with the PCBurg module (Page et al., 2020a).[4] Initial QSF18 documentation reported discrepancies between the sonic boom predictions and measurements (Page et al., 2020a; Page et al., 2020b). Figure 15 depicts the PL difference between the modeled predictions and measured boom levels in dB. The RMSE of the predictions is greater than 8 dB when compared to measurements. Several hypothesized sources of discrepancy between predictions and measurements include:

- low signal-to-noise ratio (SNR) (Anderson et al., 2024)
- not accounting for the effect of atmospheric turbulence along the propagation path through the atmospheric boundary layer (Lonzaga, 2021)
- not accounting for absorption from clouds (Baudoin et al., 2011)
- use of a simplified near-field for PCBoom modeling (the built-in F-function)
- elevated microphones (Downs et al., 2022)

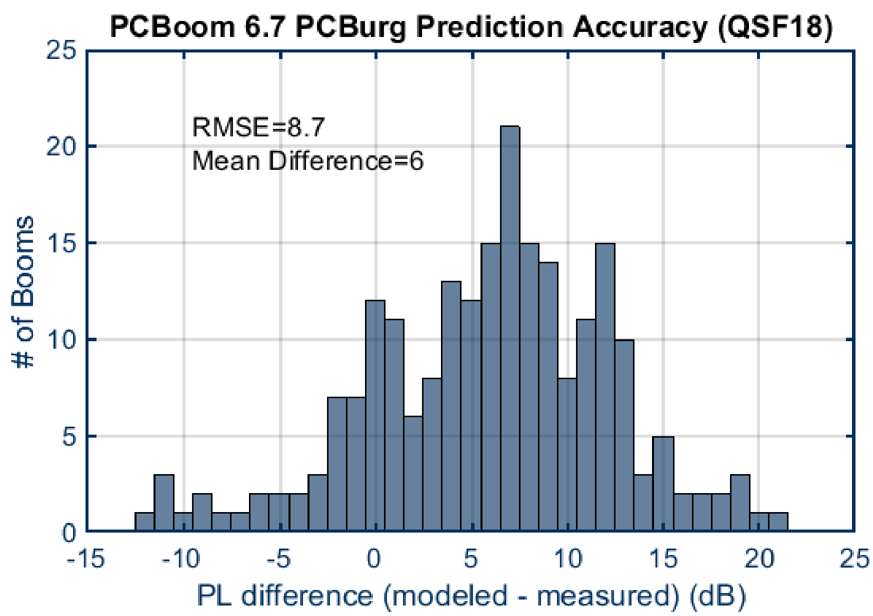

Figure 15. (From Durrant et al., 2022b) Difference between modeled and measured PL of each boom at each noise monitor from QSF18. Only measurements with signal-to-noise ratio greater than 5 dB and those within the PCBoom carpet are included, for a total of 222 measurements.

[4] At the time, the PCBurg module was the best physical model within PCBoom, though this recently gave way to the Enhanced Burgers module.

Given the discrepancies between the PCBoom predictions and measurements, Durrant et al. (2021) used an empirical model to predict PL values measured during QSF18. A simple linear model was initially used to predict PL as a function of the distance from the aircraft dive waypoint to the microphone measurement station. Results are shown in Figure 16. The coefficient of determination (R^2) for the linear fit is 0.491. For booms that were generated the same distance away from the aircraft, the measured PL varied by as much as 20 dB. The residual of the linear model is also given in Figure 16. The residual distribution appears somewhat normal (a Chi-square goodness of fit test returns a p-value of 0.27), with a standard deviation of 4.7 dB. This is the measured variability due to factors other than propagation distance.

A more thorough empirical model of the QSF18 data was then developed using many candidate predictor factors. Durrant et al. (2022b) used Lasso regression (Tibshirani, 1996) to identify a subset of nine meteorological, aircraft trajectory, and ambient factors that best described the variability of measured PL values. Ordinary least squares multiple linear regression (LSQ) using the MATLAB `fitlm` function (MathWorks, 2022a) was then performed on the data from the most significant inputs identified by Lasso regression, creating a Reduced-Order Model (ROM). This model accounted for more than 60% of the variability in the boom metrics after ambient noise was removed with a filtering method from Anderson et al. (2024).

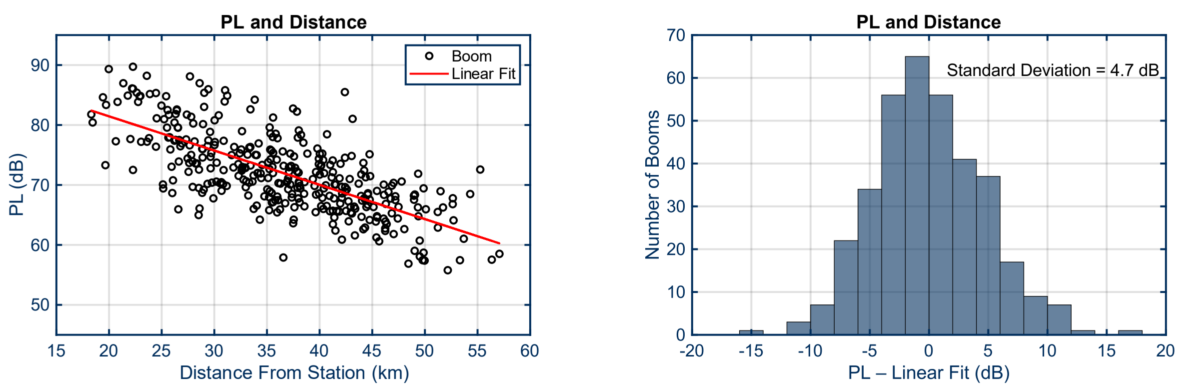

Figure 16. (From Durrant et al., 2022b) Left: A linear fit to measured levels in PL as a function of horizontal distance from the noise monitor to the F-18 dive position. Right: A histogram of PL residuals from the linear fit.

These previous regression modeling efforts with QSF18 data set the stage for the present analyses of CarpetDIEM I. The low-boom dive maneuver made the QSF18 dataset less ideal for more thorough analysis as the X-59 will make steady, level passes over communities. Additionally, the QSF18 results are expected to further differ from CarpetDIEM I results due to the use of a different version of PCBoom. The QSF18 analysis used PCBoom version 6.7 with the PCBurg module while the CarpetDIEM I analysis used the newer version 7.2 with an Enhanced Burgers propagation module (Page et al., 2020c). The latest Enhanced Burgers module includes additional physical effects related to wind effects and eliminates the need for a filtering procedure to reduce FFT-induced numerical artifacts (Lonzaga, 2019). Thus, the analysis of CarpetDIEM I data is built upon the preliminary efforts of the QSF18 analysis and utilizes the more recent PCBoom developments.

Appendix B: Propagation results using the F/A-18 F-function near-field at R/L=1
This section includes information on an additional propagation case of the CarpetDIEM I aircraft trajectories using the built-in F/A-18 F-function at R/L=1 as its near-field.

The waveform was propagated from the aircraft using the built-in F/A-18 F-function near field as input starting at a distance of one aircraft length away from the aircraft (R/L = 1) to the ground. Figure 17 shows a histogram of differences between modeled and measured metrics. The mean error and RMSE are 1.1 dB and 5.1 dB, respectively. These values are much smaller than the mean error and RMSE in PCBoom 6.7 predictions at QSF18, which were 6.0 dB and 8.7 dB, respectively.

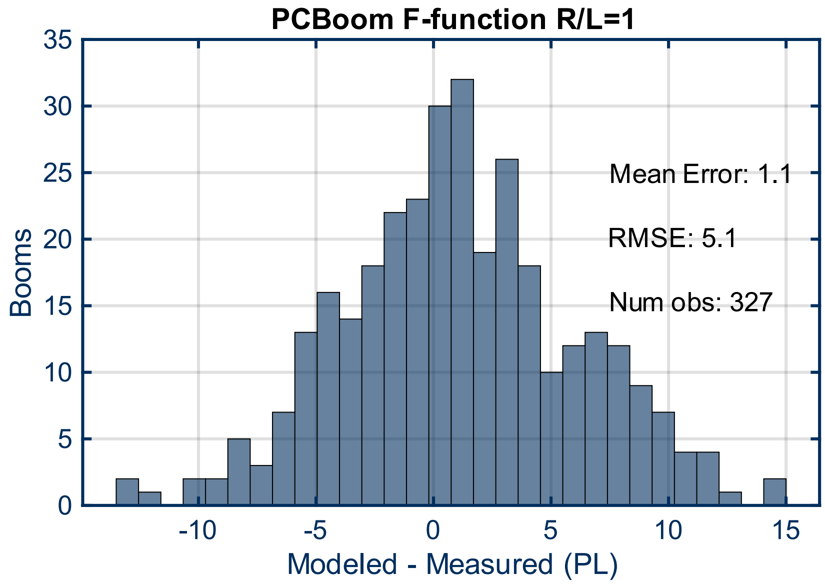

Figure 17. Differences between PCBoom-predicted PL values and measured PL values are given with PCBoom R/L set to 1. The mean error is 1.1 dB, RMSE is 5.1 dB, and there are 327 total observations.

Appendix C: Differences in predictions and measurements of other sonic boom metrics
This section contains histograms of A-, B-, D-, ESEL, and ISBAP differences between predictions and measurements in Figure 18 through Figure 22. The mean error and RMSE is tabulated for all metrics in Table 9. The predicted ASEL metric differs most from the measured ASEL, followed by PL in terms of mean error and RMSE. ISBAP and DSEL performed best followed by BSEL.

Table 9. Mean differences (error) between modeled and measured sonic boom metrics and RMSE for sonic booms generated using the F-function and CFD near-field data.

Metric	Mean Error F-function	RMSE F-function	Mean Error CFD	RMSE CFD
PL	2.0	5.3	3.2	5.9
ASEL	2.9	5.9	4.0	6.6
BSEL	1.3	4.0	2.1	4.3
DSEL	1.0	3.6	1.9	4.0
ESEL	1.9	4.6	2.8	5.1
ISBAP	0.9	4.0	1.9	4.4

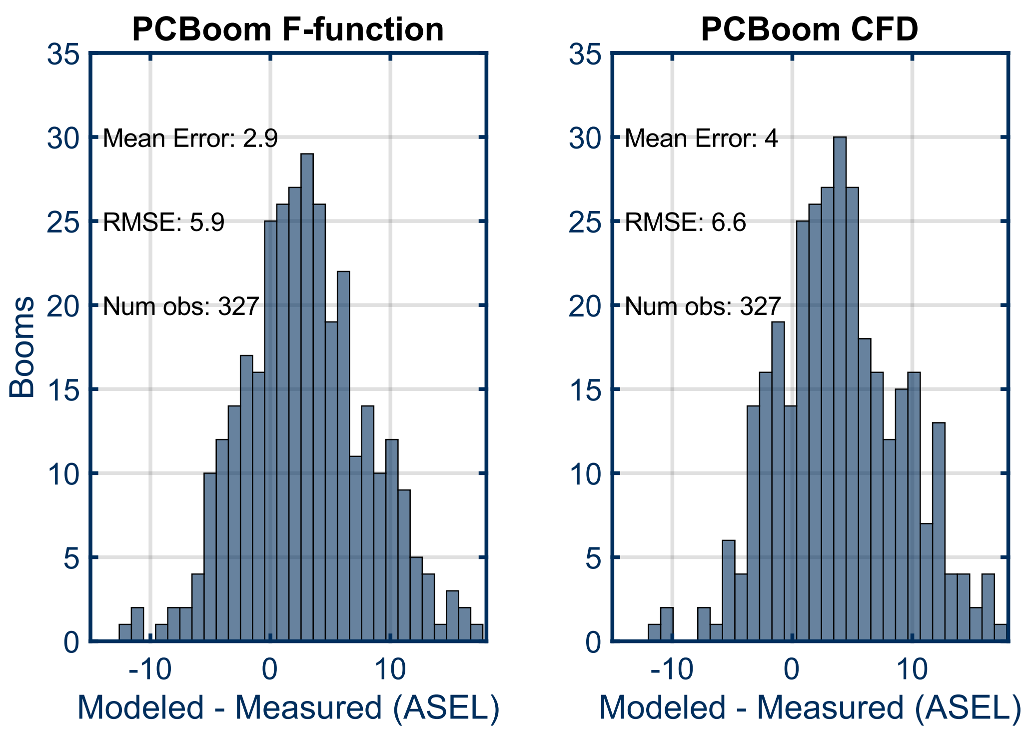

Figure 18. Differences in modeled and measured ASEL for sonic booms generated using the F-function and CFD near field data.

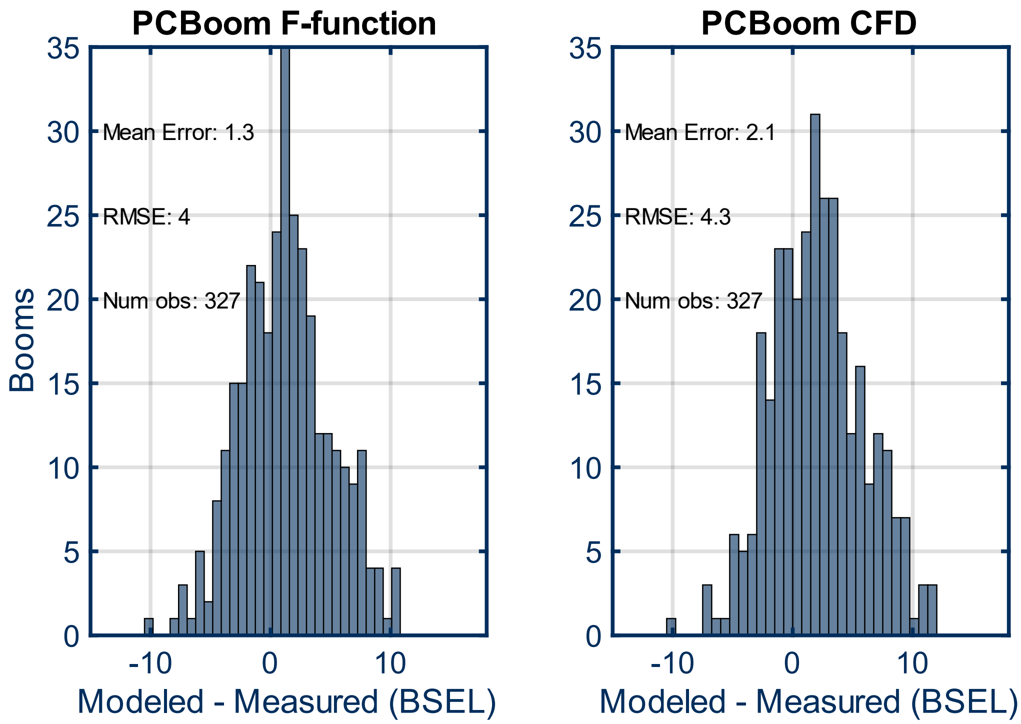

Figure 19. Differences in modeled and measured BSEL for sonic booms generated using the F-function and CFD near field data.

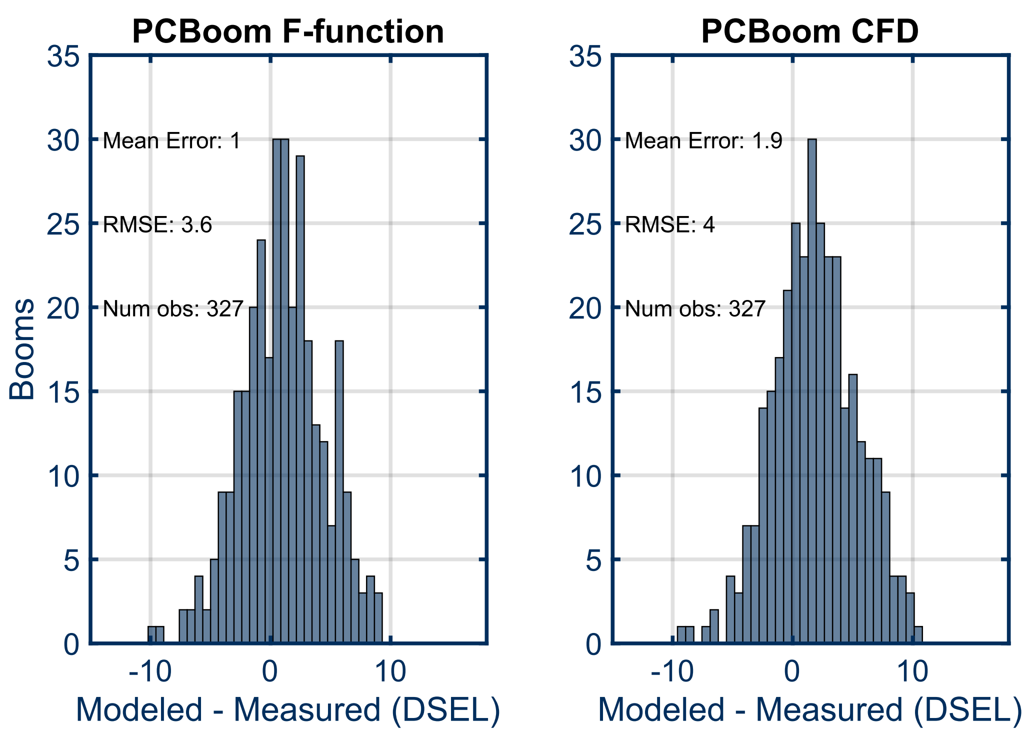

Figure 20. Differences in modeled and measured DSEL for sonic booms generated using the F-function and CFD near field data.

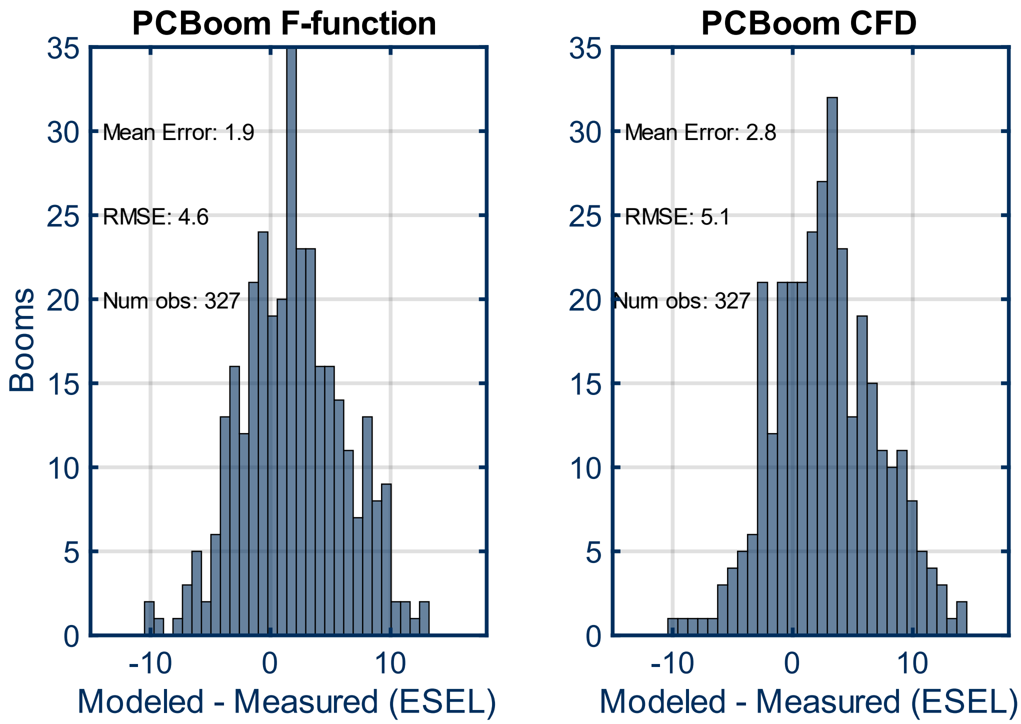

Figure 21. Differences in modeled and measured ESEL for sonic booms generated using the F-function and CFD near-field data.

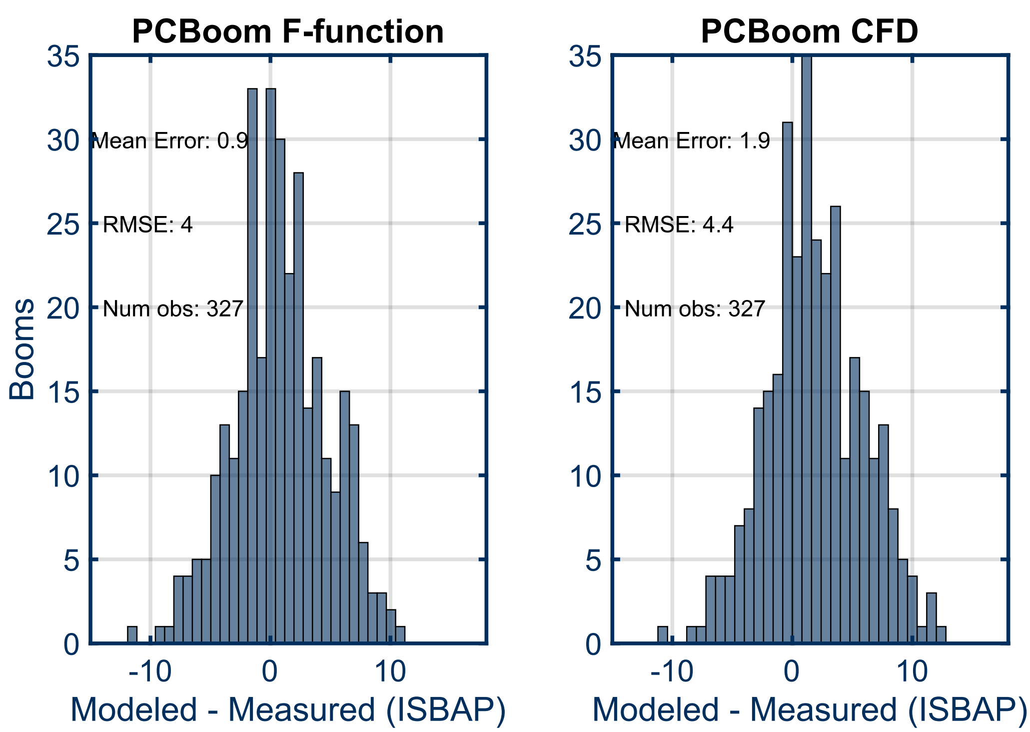

Figure 22. Differences in modeled and measured ISBAP for sonic booms generated using the F-function and CFD near-field data.

Appendix D: Lasso inputs and outputs

Tables are provided below with the inputs and outputs to Lasso regression.

Table 10. Lasso regression inputs and description

#	Input name	Description
1	Flight number	There were 6 flights at CarpetDIEM I
2	Pass number	Each flight had 4 passes, except flight 5 had 3 passes
3	Site number	The site number the measurement was made at. Attended stations for CarpetDIEM I were limited to sites 19-54.
4	Mark time	The time of day the boom was generated by the aircraft
5	Wind direction	Direction of the wind at the nearest ground weather station
6	Wind speed	Wind speed at the nearest ground weather station
7	Temperature	Temperature at the nearest ground weather station
8	Relative humidity	Relative humidity at the nearest ground weather station
9	Pressure	Atmospheric pressure at the nearest ground weather station
10	Low altitude wind direction	Wind direction at 5,000 ft. elevation for the balloon launched before that flight
11	Low altitude wind speed	Wind speed at 5,000 ft. elevation for the balloon launched before that flight
12	Low altitude temperature	Temperature at 5,000 ft. elevation for the balloon launched before that flight
13	Low altitude relative humidity	Relative humidity at 5,000 ft. elevation for the balloon launched before that flight
14	Low altitude pressure	Atmospheric pressure at 5,000 ft. elevation for the balloon launched before that flight
15	Low altitude dew point	Dew point at 5,000 ft. elevation for the balloon launched before that flight
16	High altitude wind direction	Wind direction at 30,000 ft. elevation for the balloon launched before that flight
17	High altitude wind speed	Wind speed at 30,000 ft. elevation for the balloon launched before that flight
18	High altitude temperature	Temperature at 30,000 ft. elevation for the balloon launched before that flight
19	High altitude relative humidity	Relative humidity at 30,000 ft. elevation for the balloon launched before that flight
20	High altitude pressure	Atmospheric pressure at 30,000 ft. elevation for the balloon launched before that flight
21	High altitude dew point	Dew point at 30,000 ft. elevation for the balloon launched before that flight
22	Atmospheric boundary layer height	Height of the atmospheric boundary layer from CFSv2 modeled data
23	Friction velocity	Friction velocity from CFSv2 modeled data
24	X-plane	Location of the aircraft at time of ray emission in the X-direction

25	Y-plane	Location of the aircraft at time of ray emission in the Y-direction
26	Altitude	Altitude of the aircraft at time of ray emission
27	Mach	Mach number of the aircraft at time of ray emission
28	Mach derivative	Mach number derivative of the aircraft at time of ray emission
29	Mach 2nd derivative	Mach number 2nd derivative of the aircraft at time of ray emission
30	Heading	Heading (horizontal angle) of the aircraft at time of ray emission
31	Heading derivative	Derivative of heading (horizontal angle) of the aircraft at time of ray emission
32	Heading 2nd derivative	2nd derivative of heading (horizontal angle) of the aircraft at time of ray emission
33	Flight path angle (FPA)	Angle of the aircraft in the vertical direction at time of ray emission
34	Flight path angle (FPA) derivative	Derivative of the angle of the aircraft in the vertical direction at time of ray emission
35	Flight path angle (FPA) 2nd derivative	2nd derivative of the angle of the aircraft in the vertical direction at time of ray emission
36	Weight	Weight of the aircraft at time of ray emission
37	Horizontal distance	Distance from aircraft coordinates to measurement location coordinates in the horizontal direction at time of ray emission
38	Straight-line distance	Distance from the aircraft x-y coordinates and altitude to the station x-y coordinates and altitude at time of ray emission
39	Emission angle	Angle of the emitted ray that lands closest to the given measurement station, as predicted by PCBoom
40	Emission angle squared	Squared angle of the emitted ray that lands closest to the given measurement station, as predicted by PCBoom
41	Absolute value of emission angle	Absolute value of the angle of the emitted ray that lands closest to the given measurement station, as predicted by PCBoom
42	Ambient PL	Ambient PL calculated over the 650ms immediately preceding the boom
43	Ambient ASEL	Ambient ASEL calculated over the 650ms immediately preceding the boom
44	Ambient BSEL	Ambient BSEL calculated over the 650ms immediately preceding the boom
45	Ambient DSEL	Ambient DSEL calculated over the 650ms immediately preceding the boom
46	Ambient ESEL	Ambient ESEL calculated over the 650ms immediately preceding the boom
47	Ambient ISBAP	Ambient ISBAP calculated over the 650ms immediately preceding the boom

48	Average ambient PL	Average ambient PL, calculated in 650ms windows and averaged over the 60s preceding the boom
49	Average ambient ASEL	Average ambient ASEL, calculated in 650ms windows and averaged over the 60s preceding the boom
50	Average ambient BSEL	Average ambient BSEL, calculated in 650ms windows and averaged over the 60s preceding the boom
51	Average ambient DSEL	Average ambient DSEL, calculated in 650ms windows and averaged over the 60s preceding the boom
52	Average ambient ESEL	Average ambient ESEL, calculated in 650ms windows and averaged over the 60s preceding the boom
53	Average ambient ISBAP	Average ambient ISBAP, calculated in 650ms windows and averaged over the 60s preceding the boom
54	PCBoom PL	PCBoom-modeled PL with F-function near-field input
55	PCBoom ASEL	PCBoom-modeled ASEL with F-function near-field input
56	PCBoom BSEL	PCBoom-modeled BSEL with F-function near-field input
57	PCBoom DSEL	PCBoom-modeled DSEL with F-function near-field input
58	PCBoom ESEL	PCBoom-modeled ESEL with F-function near-field input
59	PCBoom ISBAP	PCBoom-modeled ISBAP with F-function near-field input
60	PCBoom CFD PL	PCBoom-modeled PL with CFD near-field input
61	PCBoom CFD ASEL	PCBoom-modeled ASEL with CFD near-field input
62	PCBoom CFD BSEL	PCBoom-modeled BSEL with CFD near-field input
63	PCBoom CFD DSEL	PCBoom-modeled DSEL with CFD near-field input
64	PCBoom CFD ESEL	PCBoom-modeled ESEL with CFD near-field input
65	PCBoom CFD ISBAP	PCBoom-modeled ISBAP with CFD near-field input
66	PCBoom distance	Distance from the PCBoom-modeled ray landing point to the measurement station
67	PCBoom peak pressure	PCBoom-modeled peak overpressure with F-function near-field input
68	PCBoom CFD peak pressure	PCBoom-modeled peak overpressure with CFD near-field input

Table 11. Lasso regression outputs and description

#	**Output name**	**Description**
1	PL	Measured PL
2	ASEL	Measured ASEL
3	BSEL	Measured BSEL
4	DSEL	Measured DSEL
5	ESEL	Measured ESEL
6	ISBAP	Measured ISBAP
7	PCBoom ΔPM_{PL}	PCBoom-modeled PL – measured PL
8	PCBoom ΔPM_{ASEL}	PCBoom-modeled ASEL – measured ASEL
9	PCBoom ΔPM_{BSEL}	PCBoom-modeled BSEL – measured BSEL
10	PCBoom ΔPM_{DSEL}	PCBoom-modeled DSEL – measured DSEL
11	PCBoom ΔPM_{ESEL}	PCBoom-modeled ESEL – measured ESEL
12	PCBoom ΔPM_{ISBAP}	PCBoom-modeled ISBAP – measured ISBAP

Appendix E: Input Correlations

Table 12. Correlations for all inputs used in Lasso regression, with positive correlations in blue and negative correlations in red.

	Flight number	Pass number	Station number	Mark time	Wind direction	Wind speed	Temperature	Relative humidity	Pressure	Low alt. wind speed	Low alt. wind speed	Low alt. temperature	Low alt. relative humidity	Low alt. pressure	Low alt. dew point	High alt. wind direstion	High alt. wind speed	High alt. temperature	High alt. relative humidity	High alt. pressure	Hight alt. dew point	Planetary boundary layer height	Friction velocity	X-plane	Y-plane	Altitude	Mach	Mach derivative	Mach 2nd derivative	Heading	Heading derivative	Heading 2nd derivative	FPA	FPA derivative	FPA 2nd derivative	Weight	Horizontal distance	Straight-line distance	Emission angle	Emission angle squared	Abs. value of emission angle	Ambient PL	Ambient ASEL	Ambient BSEL	Ambient DSEL	Ambient ESEL	Ambient ISBAP	Avg. ambient PL	Avg. ambient ASEL	Avg. ambient BSEL	Avg. ambient DSEL	Avg. ambient ESEL	Avg. ambient ISBAP	PCBoom PL	PCBoom ASEL	PCBoom BSEL	PCBoom DSEL	PCBoom ESEL	PCBoom ISBAP	PCBoom CFD PL	PCBoom CFD ASEL	PCBoom CFD BSEL	PCBoom CFD DSEL	PCBoom CFD ESEL	PCBoom CFD ISBAP	PCBoom Distance	PCBoom peak pressure	PCBoom CFD peak pressure
Flight number	1.00	-0.05	-0.04	0.07	-0.23	0.04	0.06	-0.30	0.04	-0.47	0.06	0.88	-0.73	0.22	-0.67	-0.89	-0.46	-0.25	0.87	0.52	0.93	0.02	-0.39	0.48	0.53	0.67	0.17	0.21	0.29	0.48	0.30	0.00	-0.18	-0.20	-0.18	0.03	0.15	0.18	-0.05	-0.12	-0.12	0.15	0.14	0.26	0.18	0.17	0.22	0.09	0.09	0.19	0.10	0.10	0.13	-0.03	0.03	0.08	0.04	0.05	-0.02	-0.05	0.00	0.05	0.00	0.01	-0.04	0.14	0.14	0.10
Pass number	-0.05	1.00	0.00	0.18	0.17	0.07	0.13	-0.06	0.02	-0.09	0.03	-0.05	0.02	0.08	0.02	0.07	0.09	0.08	-0.10	0.01	-0.07	0.25	0.23	0.41	0.37	0.06	0.54	0.11	0.09	0.45	-0.23	0.23	0.07	-0.16	-0.26	-1.00	-0.02	-0.02	-0.02	-0.01	-0.01	0.01	0.01	0.00	0.00	0.01	0.00	0.02	0.02	0.03	0.04	0.03	0.04	-0.05	-0.05	-0.03	-0.04	-0.04	-0.04	-0.03	-0.03	0.00	-0.01	-0.01	-0.02	-0.04	-0.01	-0.02
Station number	-0.04	0.00	1.00	0.01	0.29	-0.29	-0.06	0.18	-0.87	0.03	0.00	-0.02	0.02	0.00	0.02	0.05	0.00	0.01	-0.04	-0.02	-0.04	0.01	0.02	-0.05	-0.06	-0.04	-0.02	-0.01	0.00	-0.02	-0.08	0.10	0.05	0.04	0.01	0.01	0.09	0.09	-0.42	-0.28	-0.20	-0.34	-0.35	-0.37	-0.35	-0.35	-0.36	-0.33	-0.34	-0.40	-0.36	-0.34	-0.38	-0.42	-0.40	-0.41	-0.41	-0.41	-0.43	-0.46	-0.45	-0.46	-0.46	-0.45	-0.47	-0.06	-0.48	-0.52
Mark time	0.07	0.18	0.01	1.00	0.47	0.38	0.92	-0.80	0.03	-0.61	0.56	0.29	-0.29	0.81	-0.17	0.25	0.03	0.64	-0.41	0.45	-0.19	0.95	0.75	0.31	0.22	0.10	0.36	-0.04	-0.18	0.31	0.09	0.10	0.15	0.18	0.15	-0.15	-0.05	-0.04	-0.01	-0.02	-0.01	-0.07	-0.07	-0.14	-0.04	-0.07	-0.09	-0.09	-0.09	-0.18	-0.06	-0.09	-0.12	-0.10	-0.04	0.01	-0.02	-0.02	-0.08	-0.13	-0.06	-0.01	-0.06	-0.06	-0.12	0.06	0.08	0.06
Wind direction	-0.23	0.17	0.29	0.47	1.00	0.08	0.39	-0.24	-0.34	-0.23	0.42	0.05	-0.15	0.49	-0.12	0.35	-0.16	0.50	-0.44	0.29	-0.26	0.52	0.41	-0.11	-0.18	-0.36	0.15	-0.12	-0.33	-0.10	-0.05	0.11	0.16	0.32	0.32	-0.13	-0.16	-0.18	-0.01	-0.10	-0.09	-0.31	-0.31	-0.43	-0.33	-0.32	-0.37	-0.26	-0.26	-0.39	-0.27	-0.27	-0.32	-0.11	-0.08	-0.05	-0.07	-0.07	-0.10	-0.14	-0.10	-0.07	-0.09	-0.09	-0.13	-0.10	-0.11	-0.13
Wind speed	0.04	0.07	-0.29	0.38	0.08	1.00	0.41	-0.50	0.30	-0.02	-0.05	0.14	-0.12	0.16	-0.01	0.20	0.00	-0.04	-0.08	-0.05	-0.13	0.33	0.40	0.10	0.08	0.07	0.34	0.10	0.06	0.11	0.06	0.09	-0.12	-0.09	-0.06	-0.05	0.03	0.04	0.16	0.18	0.16	0.20	0.20	0.22	0.24	0.20	0.24	0.24	0.24	0.29	0.28	0.24	0.30	0.07	0.07	0.08	0.08	0.07	0.08	0.09	0.10	0.11	0.10	0.09	0.09	-0.02	0.09	0.11
Temperature	0.06	0.13	-0.06	0.92	0.39	0.41	1.00	-0.85	0.12	-0.63	0.56	0.25	-0.26	0.78	-0.17	0.20	0.05	0.65	-0.39	0.46	-0.16	0.86	0.67	0.29	0.21	0.11	0.29	0.04	-0.13	0.28	0.13	0.10	0.08	0.13	0.14	-0.10	0.00	0.00	-0.03	0.05	0.07	-0.02	-0.02	-0.08	0.01	-0.01	-0.04	-0.04	-0.04	-0.13	-0.02	-0.04	-0.08	-0.11	-0.05	0.00	-0.04	-0.03	-0.09	-0.13	-0.06	-0.01	-0.06	-0.05	-0.11	0.08	0.08	0.08
Relative humidity	-0.30	-0.06	0.18	-0.80	-0.24	-0.50	-0.85	1.00	-0.15	0.50	-0.47	-0.50	0.43	-0.66	0.28	0.00	0.19	-0.42	0.09	-0.46	-0.07	-0.77	-0.47	-0.28	-0.24	-0.15	-0.36	0.03	0.18	-0.27	-0.14	0.00	-0.07	-0.16	-0.17	0.04	0.11	0.10	-0.01	0.04	0.04	-0.06	-0.07	-0.04	-0.09	-0.07	-0.06	-0.04	-0.05	-0.02	-0.08	-0.06	-0.04	-0.06	-0.12	-0.16	-0.13	-0.13	-0.08	-0.04	-0.11	-0.14	-0.10	-0.11	-0.05	-0.06	-0.20	-0.19
Pressure	0.04	0.02	-0.87	0.03	-0.34	0.30	0.12	-0.15	1.00	-0.09	0.05	0.03	-0.03	0.06	-0.05	-0.05	0.00	0.05	0.01	0.07	0.05	0.02	-0.01	0.05	0.06	0.05	-0.01	0.13	0.14	0.04	0.15	0.01	-0.15	-0.17	-0.12	-0.02	0.13	0.13	0.38	0.40	0.37	0.51	0.51	0.52	0.52	0.51	0.53	0.50	0.49	0.55	0.53	0.50	0.55	0.21	0.19	0.21	0.21	0.20	0.23	0.27	0.24	0.26	0.26	0.25	0.28	0.09	0.29	0.34
Low alt. wind speed	-0.47	-0.09	0.03	-0.61	-0.23	-0.02	-0.63	0.50	-0.09	1.00	-0.50	-0.50	0.61	-0.85	0.67	0.32	0.15	-0.53	-0.05	-0.79	-0.41	-0.50	-0.19	-0.50	-0.43	-0.44	-0.15	-0.09	-0.02	-0.49	-0.21	-0.13	-0.02	-0.10	-0.10	0.09	-0.04	-0.06	0.03	0.08	0.07	0.05	0.05	0.08	0.01	0.02	0.05	0.10	0.09	0.17	0.09	0.08	0.15	0.20	0.11	0.00	0.06	0.05	0.17	0.23	0.14	0.05	0.12	0.10	0.21	-0.11	-0.09	-0.04
Low alt. wind speed	0.06	0.03	0.00	0.56	0.42	-0.05	0.56	-0.47	0.05	-0.50	1.00	0.35	-0.28	0.73	-0.26	-0.09	-0.38	0.91	-0.28	0.78	0.08	0.71	0.06	-0.14	-0.18	-0.36	0.09	-0.22	-0.42	-0.13	0.05	0.14	0.24	0.38	0.41	0.01	-0.08	-0.09	0.05	0.00	0.01	-0.13	-0.13	-0.25	-0.16	-0.14	-0.22	-0.11	-0.11	-0.21	-0.12	-0.10	-0.18	-0.15	-0.09	-0.05	-0.08	-0.08	-0.14	-0.18	-0.11	-0.07	-0.11	-0.10	-0.17	-0.03	-0.07	-0.08
Low alt. temperature	0.88	-0.05	-0.02	0.29	0.05	0.14	0.25	-0.50	0.03	-0.50	0.35	1.00	-0.91	0.51	-0.80	-0.68	-0.76	0.02	0.66	0.74	0.82	0.32	-0.27	0.30	0.32	0.31	0.30	0.07	0.04	0.31	0.25	0.06	-0.10	0.03	0.07	0.06	0.08	0.09	0.00	-0.09	-0.08	0.09	0.08	0.16	0.11	0.11	0.14	0.06	0.06	0.13	0.08	0.07	0.10	-0.06	0.01	0.07	0.02	0.03	-0.05	-0.09	-0.02	0.03	-0.02	-0.01	-0.08	0.09	0.07	0.04
Low alt. relative humidity	-0.73	0.02	0.02	-0.29	-0.15	-0.12	-0.26	0.43	-0.03	0.61	-0.28	-0.91	1.00	-0.64	0.96	0.49	0.79	-0.07	-0.51	-0.78	-0.72	-0.28	0.20	-0.30	-0.29	-0.22	-0.30	-0.07	-0.02	-0.31	-0.20	-0.11	0.11	-0.10	-0.16	-0.04	-0.04	-0.05	-0.02	0.07	0.07	-0.05	-0.05	-0.11	-0.08	-0.07	-0.10	-0.02	-0.02	-0.07	-0.04	-0.03	-0.06	0.10	0.03	-0.05	0.01	0.00	0.09	0.13	0.06	0.00	0.05	0.04	0.11	-0.08	-0.05	-0.01
Low alt. pressure	0.22	0.08	0.00	0.81	0.49	0.16	0.78	-0.66	0.06	-0.85	0.73	0.51	-0.64	1.00	-0.62	0.01	-0.37	0.75	-0.24	0.84	0.14	0.79	0.36	0.23	0.15	-0.01	0.27	-0.07	-0.25	0.24	0.12	0.16	0.12	0.31	0.33	-0.04	-0.05	-0.05	0.03	-0.03	-0.02	-0.10	-0.10	-0.18	-0.08	-0.09	-0.13	-0.12	-0.11	-0.21	-0.10	-0.11	-0.16	-0.19	-0.10	-0.01	-0.07	-0.06	-0.16	-0.22	-0.13	-0.05	-0.12	-0.11	-0.20	0.05	0.02	-0.02
Low alt. dew point	-0.67	0.02	0.02	-0.17	-0.12	-0.01	-0.17	0.28	-0.05	0.67	-0.26	-0.80	0.96	-0.62	1.00	0.50	0.74	-0.09	-0.48	-0.79	-0.73	-0.15	0.29	-0.29	-0.27	-0.21	-0.21	-0.07	-0.03	-0.30	-0.18	-0.12	0.12	-0.11	-0.17	-0.03	-0.04	-0.05	-0.02	0.07	0.07	-0.03	-0.03	-0.08	-0.06	-0.05	-0.07	0.00	0.00	-0.03	-0.01	-0.01	-0.02	0.14	0.06	-0.03	0.03	0.02	0.12	0.16	0.09	0.02	0.08	0.06	0.14	-0.07	-0.03	0.02
High alt. wind direstion	-0.89	0.07	0.05	0.25	0.35	0.20	0.20	0.00	-0.05	0.32	-0.09	-0.68	0.49	0.01	0.50	1.00	0.39	0.22	-0.89	-0.46	-0.95	0.24	0.68	-0.31	-0.38	-0.55	0.03	-0.17	-0.27	-0.30	-0.25	0.01	0.15	0.20	0.19	-0.04	-0.15	-0.18	0.05	0.11	0.10	-0.12	-0.12	-0.23	-0.13	-0.15	-0.17	-0.08	-0.08	-0.17	-0.07	-0.10	-0.10	0.03	-0.01	-0.05	-0.02	-0.03	0.03	0.04	0.01	-0.02	0.00	-0.01	0.04	-0.10	-0.08	-0.06
High alt. wind speed	-0.46	0.09	0.00	0.03	-0.16	0.00	0.05	0.19	0.00	0.15	-0.38	-0.76	0.79	-0.37	0.74	0.39	1.00	-0.08	-0.44	-0.66	-0.59	-0.12	0.49	0.16	0.14	0.31	-0.19	0.11	0.20	0.13	-0.06	-0.10	0.04	-0.23	-0.32	-0.12	0.02	0.03	-0.07	0.02	0.02	-0.02	-0.02	-0.05	-0.01	-0.02	-0.03	-0.05	-0.04	-0.10	-0.05	-0.05	-0.08	0.06	0.01	-0.02	0.01	0.01	0.05	0.06	0.03	0.00	0.03	0.03	0.06	0.03	0.08	0.09
High alt. temperature	-0.25	0.08	0.01	0.64	0.50	-0.04	0.65	-0.42	0.05	-0.53	0.91	0.02	-0.07	0.75	-0.09	0.22	-0.08	1.00	-0.61	0.62	-0.24	0.72	0.33	-0.12	-0.19	-0.38	0.04	-0.22	-0.43	-0.12	-0.02	0.14	0.27	0.39	0.40	-0.04	-0.11	-0.12	0.04	0.02	0.03	-0.19	-0.18	-0.34	-0.21	-0.19	-0.29	-0.16	-0.16	-0.31	-0.17	-0.16	-0.25	-0.17	-0.12	-0.07	-0.10	-0.10	-0.16	-0.20	-0.14	-0.09	-0.13	-0.12	-0.18	-0.04	-0.08	-0.08
High alt. relative humidity	0.87	-0.10	-0.04	-0.41	-0.44	-0.08	-0.39	0.09	0.01	-0.05	-0.28	0.66	-0.51	-0.24	-0.48	-0.89	-0.44	-0.61	1.00	0.18	0.90	-0.42	-0.67	0.29	0.37	0.55	0.04	0.21	0.36	0.29	0.22	-0.06	-0.24	-0.29	-0.27	0.07	0.16	0.18	-0.04	-0.09	-0.10	0.18	0.18	0.34	0.20	0.20	0.27	0.14	0.14	0.29	0.14	0.15	0.21	0.05	0.07	0.08	0.07	0.07	0.05	0.04	0.06	0.06	0.05	0.06	0.04	0.10	0.09	0.07
High alt. pressure	0.52	0.01	-0.02	0.45	0.29	-0.05	0.46	-0.46	0.07	-0.79	0.78	0.74	-0.78	0.84	-0.79	-0.46	-0.66	0.62	0.18	1.00	0.57	0.51	-0.17	0.16	0.13	0.01	0.17	-0.06	-0.20	0.17	0.17	0.16	0.07	0.26	0.32	0.01	0.00	0.00	0.03	-0.06	-0.05	-0.06	-0.05	-0.09	-0.06	-0.04	-0.09	-0.07	-0.07	-0.11	-0.06	-0.06	-0.10	-0.19	-0.10	-0.01	-0.07	-0.06	-0.16	-0.22	-0.13	-0.05	-0.12	-0.10	-0.20	0.04	-0.01	-0.05
Hight alt. dew point	0.93	-0.07	-0.04	-0.19	-0.26	-0.13	-0.16	-0.07	0.05	-0.41	0.08	0.82	-0.72	0.14	-0.73	-0.95	-0.59	-0.24	0.90	0.57	1.00	-0.19	-0.65	0.33	0.39	0.50	0.06	0.17	0.24	0.33	0.25	0.02	-0.18	-0.14	-0.11	0.05	0.14	0.16	-0.03	-0.11	-0.10	0.12	0.12	0.23	0.14	0.15	0.18	0.08	0.08	0.18	0.08	0.10	0.12	-0.05	0.00	0.06	0.02	0.03	-0.04	-0.06	-0.02	0.02	-0.02	0.00	-0.06	0.10	0.08	0.04
Planetary boundary layer height	0.02	0.25	0.01	0.95	0.52	0.33	0.86	-0.77	0.02	-0.50	0.71	0.32	-0.28	0.79	-0.15	0.24	-0.12	0.72	-0.42	0.51	-0.19	1.00	0.64	0.17	0.09	-0.11	0.40	-0.11	-0.29	0.18	0.03	0.14	0.20	0.24	0.22	-0.21	-0.08	-0.08	0.02	-0.01	0.00	-0.09	-0.08	-0.17	-0.08	-0.09	-0.12	-0.08	-0.08	-0.16	-0.05	-0.08	-0.10	-0.09	-0.04	0.00	-0.03	-0.03	-0.08	-0.13	-0.06	-0.02	-0.06	-0.06	-0.12	0.01	0.02	0.00
Friction velocity	-0.39	0.23	0.02	0.75	0.41	0.40	0.67	-0.47	-0.01	-0.19	0.06	-0.27	0.20	0.36	0.29	0.68	0.49	0.33	-0.67	-0.17	-0.65	0.64	1.00	0.17	0.07	0.03	0.18	-0.02	-0.09	0.16	-0.04	0.00	0.14	0.06	0.00	-0.21	-0.07	-0.06	-0.01	0.03	0.03	-0.08	-0.08	-0.14	-0.04	-0.08	-0.08	-0.08	-0.08	-0.18	-0.06	-0.09	-0.10	0.00	0.00	0.00	0.00	0.00	0.00	-0.02	0.00	0.01	0.00	-0.01	-0.01	0.02	0.06	0.06
X-plane	0.48	0.41	-0.05	0.31	-0.11	0.10	0.29	-0.28	0.05	-0.50	-0.14	0.30	-0.30	0.23	-0.29	-0.31	0.16	-0.12	0.29	0.16	0.33	0.17	0.17	1.00	0.98	0.71	0.31	0.29	0.31	0.98	0.04	0.09	-0.05	-0.28	-0.38	-0.44	0.01	0.04	-0.09	-0.19	-0.16	0.11	0.11	0.18	0.17	0.14	0.18	0.04	0.04	0.05	0.06	0.05	0.05	0.06	0.10	0.17	0.14	0.14	0.09	0.06	0.09	0.16	0.12	0.12	0.08	0.20	0.31	0.28
Y-plane	0.53	0.37	-0.06	0.22	-0.18	0.08	0.21	-0.24	0.06	-0.43	-0.18	0.32	-0.29	0.15	-0.27	-0.38	0.14	-0.19	0.37	0.13	0.39	0.09	0.07	0.98	1.00	0.73	0.29	0.28	0.34	0.96	0.07	0.06	-0.06	-0.32	-0.41	-0.40	0.04	0.07	-0.09	-0.18	-0.16	0.14	0.13	0.21	0.19	0.16	0.21	0.06	0.06	0.09	0.08	0.07	0.08	0.09	0.13	0.19	0.16	0.16	0.11	0.09	0.12	0.18	0.14	0.14	0.11	0.22	0.32	0.29
Altitude	0.67	0.06	-0.04	0.10	-0.36	0.07	0.11	-0.15	0.05	-0.44	-0.36	0.31	-0.22	-0.01	-0.21	-0.55	0.31	-0.38	0.55	0.01	0.50	-0.11	0.03	0.71	0.73	1.00	0.08	0.36	0.53	0.69	0.25	-0.04	-0.20	-0.43	-0.48	-0.11	0.21	0.25	-0.10	-0.08	-0.08	0.13	0.13	0.25	0.19	0.17	0.23	0.05	0.05	0.11	0.07	0.06	0.08	-0.02	0.01	0.06	0.03	0.04	-0.01	-0.03	0.00	0.03	0.00	0.01	-0.03	0.19	0.20	0.17
Mach	0.17	0.54	-0.02	0.36	0.15	0.34	0.29	-0.36	-0.01	-0.15	0.09	0.30	-0.30	0.27	-0.21	0.03	-0.19	0.04	0.04	0.17	0.06	0.40	0.18	0.31	0.29	0.08	1.00	0.08	-0.06	0.35	-0.03	0.18	-0.17	-0.07	-0.03	-0.53	-0.13	-0.12	0.02	-0.03	-0.01	0.03	0.03	0.03	0.04	0.03	0.03	0.08	0.08	0.11	0.11	0.08	0.13	-0.02	0.01	0.03	0.01	0.02	-0.01	-0.02	0.01	0.03	0.01	0.01	-0.02	-0.12	0.05	0.02
Mach Derivative	0.21	0.11	-0.01	-0.04	-0.12	0.10	0.04	0.03	0.13	-0.09	-0.22	0.07	-0.07	-0.07	-0.07	-0.17	0.11	-0.22	0.21	-0.06	0.17	-0.11	-0.02	0.29	0.28	0.36	0.08	1.00	0.71	0.38	0.23	0.43	-0.72	-0.79	-0.62	-0.12	0.47	0.47	0.01	0.48	0.53	0.08	0.06	0.17	0.10	0.08	0.16	0.05	0.03	0.13	0.07	0.04	0.13	-0.14	-0.14	-0.11	-0.13	-0.13	-0.13	-0.06	-0.07	-0.05	-0.06	-0.06	-0.05	0.08	-0.08	-0.01
Mach 2nd Derivative	0.29	0.09	0.00	-0.18	-0.33	0.06	-0.13	0.18	0.14	-0.02	-0.42	0.04	-0.02	-0.25	-0.03	-0.27	0.20	-0.43	0.36	-0.20	0.24	-0.29	-0.09	0.31	0.34	0.53	-0.06	0.71	1.00	0.40	0.22	0.38	-0.50	-0.84	-0.86	-0.11	0.75	0.76	-0.04	0.59	0.57	0.05	0.03	0.20	0.10	0.06	0.17	-0.01	-0.03	0.11	0.01	-0.01	0.08	-0.35	-0.37	-0.36	-0.36	-0.37	-0.34	-0.28	-0.32	-0.31	-0.30	-0.31	-0.28	0.19	-0.28	-0.22
Heading	0.48	0.45	-0.02	0.31	-0.10	0.11	0.28	-0.27	0.04	-0.49	-0.13	0.31	-0.31	0.24	-0.30	-0.30	0.13	-0.12	0.29	0.17	0.33	0.18	0.16	0.98	0.96	0.69	0.35	0.38	0.40	1.00	-0.01	0.25	-0.10	-0.38	-0.48	-0.47	0.09	0.12	-0.09	-0.11	-0.10	0.09	0.09	0.15	0.14	0.11	0.15	0.02	0.02	0.04	0.04	0.03	0.04	-0.02	0.02	0.09	0.05	0.05	0.00	-0.01	0.02	0.08	0.04	0.05	0.01	0.17	0.21	0.19
Heading derivative	0.30	-0.23	-0.08	0.09	-0.05	0.06	0.13	-0.14	0.15	-0.21	0.05	0.25	-0.20	0.12	-0.18	-0.25	-0.06	-0.02	0.22	0.17	0.25	0.03	-0.04	0.04	0.07	0.25	-0.03	0.23	0.22	-0.01	1.00	-0.15	-0.28	-0.20	-0.09	0.22	0.33	0.33	0.03	0.35	0.38	0.07	0.06	0.18	0.13	0.10	0.17	0.01	0.00	0.09	0.03	0.02	0.07	-0.12	-0.10	-0.09	-0.10	-0.10	-0.11	-0.11	-0.09	-0.09	-0.10	-0.10	-0.10	0.34	0.10	0.13
Heading 2nd derivative	0.00	0.23	0.10	0.10	0.11	0.09	0.10	0.00	0.01	-0.13	0.14	0.06	-0.11	0.16	-0.12	0.01	-0.10	0.14	-0.06	0.16	0.02	0.14	0.00	0.09	0.06	-0.04	0.18	0.43	0.38	0.25	-0.15	1.00	-0.31	-0.40	-0.39	-0.21	0.35	0.35	-0.01	0.34	0.33	-0.10	-0.11	-0.11	-0.12	-0.11	-0.11	-0.08	-0.09	-0.08	-0.08	-0.09	-0.08	-0.43	-0.42	-0.39	-0.41	-0.41	-0.43	-0.39	-0.38	-0.35	-0.37	-0.37	-0.38	-0.12	-0.43	-0.40
FPA	-0.18	0.07	0.05	0.15	0.16	-0.12	0.08	-0.07	-0.15	-0.02	0.24	-0.10	0.11	0.12	0.12	0.15	0.04	0.27	-0.24	0.07	-0.18	0.20	0.14	-0.05	-0.06	-0.20	-0.17	-0.72	-0.50	-0.10	-0.28	-0.31	1.00	0.70	0.41	-0.06	-0.34	-0.33	-0.05	-0.47	-0.53	-0.11	-0.09	-0.20	-0.13	-0.11	-0.18	-0.11	-0.09	-0.21	-0.13	-0.11	-0.20	0.10	0.10	0.09	0.10	0.10	0.09	0.03	0.05	0.05	0.05	0.05	0.03	0.02	0.05	-0.01
FPA derivative	-0.20	-0.16	0.04	0.18	0.32	-0.09	0.13	-0.16	-0.17	-0.10	0.38	0.03	-0.10	0.31	-0.11	0.20	-0.23	0.39	-0.29	0.26	-0.14	0.24	0.06	-0.28	-0.32	-0.43	-0.07	-0.79	-0.84	-0.38	-0.20	-0.40	0.70	1.00	0.92	0.18	-0.61	-0.62	0.00	-0.57	-0.57	-0.09	-0.07	-0.22	-0.12	-0.10	-0.20	-0.04	-0.02	-0.16	-0.06	-0.04	-0.13	0.17	0.20	0.20	0.19	0.20	0.16	0.08	0.12	0.12	0.11	0.12	0.07	-0.14	0.14	0.06
FPA 2nd derivative	-0.18	-0.26	0.01	0.15	0.32	-0.06	0.14	-0.17	-0.12	-0.10	0.41	0.07	-0.16	0.33	-0.17	0.19	-0.32	0.40	-0.27	0.32	-0.11	0.22	0.00	-0.38	-0.41	-0.48	-0.03	-0.62	-0.86	-0.48	-0.09	-0.39	0.41	0.92	1.00	0.28	-0.64	-0.66	0.05	-0.49	-0.45	-0.04	-0.03	-0.18	-0.09	-0.06	-0.15	0.01	0.02	-0.10	-0.01	0.01	-0.07	0.22	0.25	0.26	0.24	0.25	0.21	0.14	0.19	0.19	0.17	0.19	0.14	-0.18	0.19	0.12
Weight	0.03	-1.00	0.01	-0.15	-0.13	-0.05	-0.10	0.04	-0.02	0.09	0.01	0.06	-0.04	-0.04	-0.03	-0.04	-0.12	-0.04	0.07	0.01	0.05	-0.21	-0.21	-0.44	-0.40	-0.11	-0.53	-0.12	-0.11	-0.47	0.22	-0.21	-0.06	0.18	0.28	1.00	0.03	0.02	0.02	0.03	0.03	-0.01	-0.02	-0.01	-0.01	-0.01	-0.01	-0.03	-0.03	-0.03	-0.04	-0.03	-0.04	0.04	0.03	0.01	0.02	0.02	0.03	0.01	0.01	-0.01	0.00	0.00	0.00	0.04	-0.02	0.00
Horizontal distance	0.15	-0.02	0.09	-0.05	-0.16	0.03	0.00	0.11	0.13	-0.04	-0.08	0.08	-0.04	-0.05	-0.04	-0.15	0.02	-0.11	0.16	0.00	0.14	-0.08	-0.07	0.01	0.04	0.21	-0.13	0.47	0.75	0.09	0.33	0.35	-0.34	-0.61	-0.64	0.03	1.00	1.00	-0.11	0.81	0.78	-0.02	-0.04	0.12	0.04	0.00	0.11	-0.10	-0.11	0.01	-0.08	-0.10	-0.01	-0.78	-0.80	-0.80	-0.80	-0.81	-0.77	-0.72	-0.75	-0.76	-0.75	-0.76	-0.71	0.31	-0.58	-0.52
Straight-line distance	0.18	-0.02	0.09	-0.04	-0.18	0.04	0.00	0.10	0.13	-0.06	-0.09	0.09	-0.05	-0.05	-0.05	-0.18	0.03	-0.12	0.18	0.00	0.16	-0.08	-0.06	0.04	0.07	0.25	-0.12	0.47	0.76	0.12	0.33	0.35	-0.33	-0.62	-0.66	0.02	1.00	1.00	-0.11	0.80	0.76	-0.01	-0.03	0.13	0.05	0.01	0.12	-0.09	-0.11	0.01	-0.07	-0.09	-0.01	-0.77	-0.80	-0.80	-0.79	-0.80	-0.77	-0.72	-0.75	-0.75	-0.74	-0.75	-0.71	0.31	-0.57	-0.51
Emission angle	-0.05	-0.02	-0.42	-0.01	-0.01	0.16	-0.03	-0.01	0.38	0.03	0.05	0.00	-0.02	0.03	-0.02	0.05	-0.07	0.04	-0.04	0.03	-0.03	0.02	-0.01	-0.09	-0.09	-0.10	0.02	0.01	-0.04	-0.09	0.03	-0.01	-0.05	0.00	0.05	0.02	-0.11	-0.11	1.00	0.10	0.05	0.11	0.11	0.07	0.09	0.08	0.09	0.14	0.14	0.13	0.15	0.13	0.16	0.31	0.30	0.31	0.31	0.31	0.32	0.33	0.33	0.34	0.34	0.34	0.34	-0.11	0.16	0.18
Emission angle squared	-0.12	-0.01	-0.28	-0.02	-0.10	0.18	0.05	0.04	0.40	0.08	0.00	-0.09	0.07	-0.03	0.07	0.11	0.02	0.02	-0.09	-0.06	-0.11	-0.01	0.03	-0.19	-0.18	-0.08	-0.03	0.48	0.59	-0.11	0.35	0.34	-0.47	-0.57	-0.49	0.03	0.81	0.80	0.10	1.00	0.96	0.03	0.01	0.14	0.07	0.04	0.13	-0.01	-0.03	0.10	0.02	-0.01	0.09	-0.47	-0.51	-0.52	-0.51	-0.52	-0.47	-0.39	-0.43	-0.44	-0.43	-0.44	-0.38	0.20	-0.37	-0.28
Abs. value of emission angle	-0.12	-0.01	-0.20	-0.01	-0.09	0.16	0.07	0.04	0.37	0.07	0.01	-0.08	0.07	-0.02	0.07	0.10	0.02	0.03	-0.10	-0.05	-0.10	0.00	0.03	-0.16	-0.16	-0.08	-0.01	0.53	0.57	-0.10	0.38	0.33	-0.53	-0.57	-0.45	0.03	0.78	0.76	0.05	0.96	1.00	0.11	0.09	0.20	0.16	0.12	0.21	0.08	0.06	0.17	0.11	0.08	0.18	-0.46	-0.49	-0.49	-0.49	-0.49	-0.45	-0.38	-0.42	-0.43	-0.42	-0.43	-0.38	0.19	-0.37	-0.28
Ambient PL	0.15	0.01	-0.34	-0.07	-0.31	0.20	-0.02	-0.06	0.51	0.05	-0.13	0.09	-0.05	-0.10	-0.03	-0.12	-0.02	-0.19	0.18	-0.06	0.12	-0.09	-0.08	0.11	0.14	0.13	0.03	0.08	0.05	0.09	0.07	-0.10	-0.11	-0.09	-0.04	-0.01	-0.02	-0.01	0.11	0.03	0.11	1.00	1.00	0.91	0.97	0.99	0.94	0.94	0.93	0.89	0.93	0.94	0.91	0.23	0.22	0.21	0.22	0.22	0.24	0.23	0.22	0.21	0.22	0.22	0.24	0.10	0.27	0.27
Ambient ASEL	0.14	0.01	-0.35	-0.07	-0.31	0.20	-0.02	-0.07	0.51	0.05	-0.13	0.08	-0.05	-0.10	-0.03	-0.12	-0.02	-0.18	0.18	-0.05	0.12	-0.08	-0.08	0.11	0.13	0.13	0.03	0.06	0.03	0.09	0.06	-0.11	-0.09	-0.07	-0.03	-0.02	-0.04	-0.03	0.11	0.01	0.09	1.00	1.00	0.90	0.97	0.99	0.93	0.94	0.94	0.89	0.94	0.94	0.91	0.24	0.22	0.22	0.23	0.22	0.25	0.24	0.22	0.22	0.23	0.22	0.24	0.09	0.28	0.28
Ambient BSEL	0.26	0.00	-0.37	-0.14	-0.43	0.22	-0.08	-0.04	0.52	0.08	-0.25	0.16	-0.11	-0.18	-0.08	-0.23	-0.05	-0.34	0.34	-0.09	0.23	-0.17	-0.14	0.18	0.21	0.25	0.03	0.17	0.20	0.15	0.18	-0.11	-0.20	-0.22	-0.18	-0.01	0.12	0.13	0.07	0.14	0.20	0.91	0.90	1.00	0.96	0.94	0.98	0.78	0.77	0.86	0.80	0.79	0.84	0.21	0.18	0.18	0.19	0.18	0.21	0.22	0.20	0.19	0.20	0.19	0.22	0.23	0.29	0.30
Ambient DSEL	0.18	0.00	-0.35	-0.04	-0.33	0.24	0.01	-0.09	0.52	0.01	-0.16	0.11	-0.08	-0.08	-0.06	-0.13	-0.01	-0.21	0.20	-0.06	0.14	-0.08	-0.04	0.17	0.19	0.19	0.04	0.10	0.10	0.14	0.13	-0.12	-0.13	-0.12	-0.09	-0.01	0.04	0.05	0.09	0.07	0.16	0.97	0.97	0.96	1.00	0.99	0.98	0.87	0.87	0.86	0.88	0.88	0.87	0.22	0.21	0.20	0.21	0.21	0.23	0.22	0.21	0.20	0.21	0.21	0.23	0.18	0.30	0.30
Ambient ESEL	0.17	0.01	-0.35	-0.07	-0.32	0.20	-0.01	-0.07	0.51	0.02	-0.14	0.11	-0.07	-0.09	-0.05	-0.15	-0.02	-0.19	0.20	-0.04	0.15	-0.09	-0.08	0.14	0.16	0.17	0.03	0.08	0.06	0.11	0.10	-0.11	-0.11	-0.10	-0.06	-0.01	0.00	0.01	0.08	0.04	0.12	0.99	0.99	0.94	0.99	1.00	0.95	0.92	0.91	0.88	0.92	0.92	0.90	0.23	0.21	0.21	0.22	0.21	0.23	0.23	0.21	0.21	0.22	0.21	0.23	0.14	0.30	0.29
Ambient ISBAP	0.22	0.00	-0.36	-0.09	-0.37	0.24	-0.04	-0.06	0.53	0.05	-0.22	0.14	-0.10	-0.13	-0.07	-0.17	-0.03	-0.29	0.27	-0.09	0.18	-0.12	-0.08	0.18	0.21	0.23	0.03	0.16	0.17	0.15	0.17	-0.11	-0.18	-0.20	-0.15	-0.01	0.11	0.12	0.09	0.13	0.21	0.94	0.93	0.98	0.98	0.95	1.00	0.81	0.81	0.85	0.83	0.82	0.86	0.21	0.19	0.19	0.20	0.19	0.22	0.22	0.20	0.19	0.21	0.20	0.22	0.21	0.29	0.29
Avg. ambient PL	0.09	0.02	-0.33	-0.09	-0.26	0.24	-0.04	-0.04	0.50	0.10	-0.11	0.06	-0.02	-0.12	0.00	-0.08	-0.05	-0.16	0.14	-0.07	0.08	-0.08	-0.08	0.04	0.06	0.05	0.08	0.05	-0.01	0.02	0.01	-0.08	-0.11	-0.04	0.01	-0.03	-0.10	-0.09	0.14	-0.01	0.08	0.94	0.94	0.78	0.87	0.92	0.81	1.00	1.00	0.94	0.99	1.00	0.97	0.23	0.21	0.21	0.22	0.21	0.24	0.23	0.22	0.21	0.22	0.22	0.24	-0.03	0.22	0.22
Avg. ambient ASEL	0.09	0.02	-0.34	-0.09	-0.26	0.24	-0.04	-0.05	0.49	0.09	-0.11	0.06	-0.02	-0.11	0.00	-0.08	-0.04	-0.16	0.14	-0.07	0.08	-0.08	-0.08	0.04	0.06	0.05	0.08	0.03	-0.03	0.02	0.00	-0.09	-0.09	-0.02	0.02	-0.03	-0.11	-0.11	0.14	-0.03	0.06	0.93	0.94	0.77	0.87	0.91	0.81	1.00	1.00	0.93	0.99	1.00	0.96	0.24	0.22	0.22	0.23	0.22	0.24	0.24	0.23	0.22	0.23	0.22	0.24	-0.04	0.23	0.23
Avg. ambient BSEL	0.19	0.03	-0.40	-0.18	-0.39	0.29	-0.13	-0.02	0.55	0.17	-0.21	0.13	-0.07	-0.21	-0.03	-0.17	-0.10	-0.31	0.29	-0.11	0.18	-0.16	-0.18	0.05	0.09	0.11	0.11	0.13	0.11	0.04	0.09	-0.08	-0.21	-0.16	-0.10	-0.03	0.01	0.01	0.13	0.10	0.17	0.89	0.89	0.86	0.86	0.88	0.85	0.94	0.93	1.00	0.95	0.94	0.98	0.21	0.19	0.17	0.19	0.18	0.21	0.23	0.21	0.19	0.21	0.20	0.23	0.03	0.22	0.24
Avg. ambient DSEL	0.10	0.04	-0.36	-0.06	-0.27	0.28	-0.02	-0.08	0.53	0.09	-0.12	0.08	-0.04	-0.10	-0.01	-0.07	-0.05	-0.17	0.14	-0.06	0.08	-0.05	-0.06	0.06	0.08	0.07	0.11	0.07	0.01	0.04	0.03	-0.08	-0.13	-0.06	-0.01	-0.04	-0.08	-0.07	0.15	0.02	0.11	0.93	0.94	0.80	0.88	0.92	0.83	0.99	0.99	0.95	1.00	0.99	0.98	0.23	0.21	0.21	0.22	0.21	0.23	0.24	0.22	0.21	0.23	0.22	0.24	-0.02	0.23	0.24
Avg. ambient ESEL	0.10	0.03	-0.34	-0.09	-0.27	0.24	-0.04	-0.06	0.50	0.08	-0.10	0.07	-0.03	-0.11	-0.01	-0.10	-0.05	-0.16	0.15	-0.06	0.10	-0.08	-0.09	0.05	0.07	0.06	0.08	0.04	-0.01	0.03	0.02	-0.09	-0.11	-0.04	0.01	-0.03	-0.10	-0.09	0.13	-0.01	0.08	0.94	0.94	0.79	0.88	0.92	0.82	1.00	1.00	0.94	0.99	1.00	0.97	0.23	0.22	0.21	0.22	0.22	0.24	0.24	0.22	0.21	0.23	0.22	0.24	-0.02	0.23	0.23
Avg. ambient ISBAP	0.13	0.04	-0.38	-0.12	-0.32	0.30	-0.08	-0.04	0.55	0.15	-0.18	0.10	-0.06	-0.16	-0.02	-0.10	-0.08	-0.25	0.21	-0.10	0.12	-0.10	-0.10	0.05	0.08	0.08	0.13	0.13	0.08	0.04	0.07	-0.08	-0.20	-0.13	-0.07	-0.04	-0.01	-0.01	0.16	0.09	0.18	0.91	0.91	0.84	0.87	0.90	0.86	0.97	0.96	0.98	0.98	0.97	1.00	0.22	0.19	0.18	0.20	0.19	0.22	0.23	0.21	0.20	0.21	0.20	0.23	0.00	0.21	0.23
PCBoom PL	-0.03	-0.05	-0.42	-0.10	-0.11	0.07	-0.11	-0.06	0.21	0.20	-0.15	-0.06	0.10	-0.19	0.14	0.03	0.06	-0.17	0.05	-0.19	-0.05	-0.09	0.00	0.06	0.09	-0.02	-0.02	-0.14	-0.35	-0.02	-0.12	-0.43	0.10	0.17	0.22	0.04	-0.78	-0.77	0.31	-0.47	-0.46	0.23	0.24	0.21	0.22	0.23	0.21	0.23	0.24	0.21	0.23	0.23	0.22	1.00	0.99	0.98	0.99	0.99	1.00	0.99	0.99	0.97	0.98	0.98	0.98	-0.09	0.96	0.95
PCBoom ASEL	0.03	-0.05	-0.40	-0.04	-0.08	0.07	-0.05	-0.12	0.19	0.11	-0.09	0.01	0.03	-0.10	0.06	-0.01	0.01	-0.12	0.07	-0.10	0.00	-0.04	0.00	0.10	0.13	0.01	0.01	-0.14	-0.37	0.02	-0.10	-0.42	0.10	0.20	0.25	0.03	-0.80	-0.80	0.30	-0.51	-0.49	0.22	0.22	0.18	0.21	0.21	0.19	0.21	0.22	0.19	0.21	0.22	0.19	0.99	1.00	0.99	1.00	1.00	0.99	0.97	0.99	0.98	0.98	0.99	0.97	-0.09	0.97	0.96
PCBoom BSEL	0.08	-0.03	-0.41	0.01	-0.05	0.08	0.00	-0.16	0.21	0.00	-0.05	0.07	-0.05	-0.01	-0.03	-0.05	-0.02	-0.07	0.08	-0.01	0.06	0.00	0.00	0.17	0.19	0.06	0.03	-0.11	-0.36	0.09	-0.09	-0.39	0.09	0.20	0.26	0.01	-0.80	-0.80	0.31	-0.52	-0.49	0.21	0.22	0.18	0.20	0.21	0.19	0.21	0.22	0.17	0.21	0.21	0.18	0.98	0.99	1.00	1.00	1.00	0.98	0.96	0.98	0.99	0.98	0.98	0.96	-0.09	0.98	0.96
PCBoom DSEL	0.04	-0.04	-0.41	-0.02	-0.07	0.08	-0.04	-0.13	0.21	0.06	-0.08	0.02	0.01	-0.07	0.03	-0.02	0.01	-0.10	0.07	-0.07	0.02	-0.03	0.00	0.14	0.16	0.03	0.01	-0.13	-0.36	0.05	-0.10	-0.41	0.10	0.19	0.24	0.02	-0.80	-0.79	0.31	-0.51	-0.49	0.22	0.23	0.19	0.21	0.22	0.20	0.22	0.23	0.19	0.22	0.22	0.20	0.99	1.00	1.00	1.00	1.00	0.99	0.97	0.98	0.99	0.99	0.99	0.97	-0.09	0.98	0.97
PCBoom ESEL	0.05	-0.04	-0.41	-0.02	-0.07	0.07	-0.03	-0.13	0.20	0.05	-0.08	0.03	0.00	-0.06	0.02	-0.03	0.01	-0.10	0.07	-0.06	0.03	-0.03	0.00	0.14	0.16	0.04	0.02	-0.13	-0.37	0.05	-0.10	-0.41	0.10	0.20	0.25	0.02	-0.81	-0.80	0.31	-0.52	-0.49	0.22	0.22	0.18	0.21	0.21	0.19	0.21	0.22	0.18	0.21	0.22	0.19	0.99	1.00	1.00	1.00	1.00	0.99	0.97	0.98	0.99	0.98	0.99	0.97	-0.09	0.98	0.96
PCBoom ISBAP	-0.02	-0.04	-0.43	-0.08	-0.10	0.08	-0.09	-0.08	0.23	0.17	-0.14	-0.05	0.09	-0.16	0.12	0.03	0.05	-0.16	0.05	-0.16	-0.04	-0.08	0.00	0.09	0.11	-0.01	-0.01	-0.13	-0.34	0.00	-0.11	-0.43	0.09	0.16	0.21	0.03	-0.77	-0.77	0.32	-0.47	-0.45	0.24	0.25	0.21	0.23	0.23	0.22	0.24	0.24	0.21	0.23	0.24	0.22	1.00	0.99	0.98	0.99	0.99	1.00	0.99	0.99	0.98	0.99	0.99	0.99	-0.09	0.96	0.96
PCBoom CFD PL	-0.05	-0.03	-0.46	-0.13	-0.14	0.09	-0.13	-0.04	0.27	0.23	-0.18	-0.09	0.13	-0.22	0.16	0.04	0.06	-0.20	0.04	-0.22	-0.06	-0.13	-0.02	0.06	0.09	-0.03	-0.02	-0.06	-0.28	-0.01	-0.11	-0.39	0.03	0.08	0.14	0.01	-0.72	-0.72	0.33	-0.39	-0.38	0.23	0.24	0.22	0.22	0.23	0.22	0.23	0.24	0.23	0.24	0.24	0.23	0.99	0.97	0.96	0.97	0.97	0.99	1.00	0.99	0.98	0.99	0.99	1.00	-0.08	0.93	0.96
PCBoom CFD ASEL	0.00	-0.03	-0.45	-0.06	-0.10	0.10	-0.06	-0.11	0.24	0.14	-0.11	-0.02	0.06	-0.13	0.09	0.01	0.03	-0.14	0.06	-0.13	-0.02	-0.06	0.00	0.09	0.12	0.00	0.01	-0.07	-0.32	0.02	-0.09	-0.38	0.05	0.12	0.19	0.01	-0.75	-0.75	0.33	-0.43	-0.42	0.22	0.22	0.20	0.21	0.21	0.20	0.22	0.23	0.21	0.22	0.22	0.21	0.99	0.99	0.98	0.98	0.98	0.99	0.99	1.00	0.99	1.00	1.00	0.99	-0.07	0.95	0.97
PCBoom CFD BSEL	0.05	0.00	-0.46	-0.01	-0.07	0.11	-0.01	-0.14	0.26	0.05	-0.07	0.03	0.00	-0.05	0.02	-0.02	0.00	-0.09	0.06	-0.05	0.02	-0.02	0.01	0.16	0.18	0.03	0.03	-0.05	-0.31	0.08	-0.09	-0.35	0.05	0.12	0.19	-0.01	-0.76	-0.75	0.34	-0.44	-0.43	0.21	0.22	0.19	0.20	0.21	0.19	0.21	0.22	0.19	0.21	0.21	0.20	0.97	0.98	0.99	0.99	0.99	0.98	0.98	0.99	1.00	1.00	1.00	0.98	-0.07	0.97	0.98
PCBoom CFD DSEL	0.00	-0.01	-0.46	-0.06	-0.09	0.10	-0.06	-0.10	0.26	0.12	-0.11	-0.02	0.05	-0.12	0.08	0.00	0.03	-0.13	0.05	-0.12	-0.02	-0.06	0.00	0.12	0.14	0.00	0.01	-0.06	-0.30	0.04	-0.10	-0.37	0.05	0.11	0.17	0.00	-0.75	-0.74	0.34	-0.43	-0.42	0.22	0.23	0.20	0.21	0.22	0.21	0.22	0.23	0.21	0.23	0.23	0.21	0.98	0.98	0.98	0.99	0.98	0.99	0.99	1.00	1.00	1.00	1.00	0.99	-0.07	0.96	0.98
PCBoom CFD ESEL	0.01	-0.01	-0.45	-0.06	-0.09	0.09	-0.05	-0.11	0.25	0.10	-0.10	-0.01	0.04	-0.11	0.06	-0.01	0.03	-0.12	0.06	-0.10	0.00	-0.06	-0.01	0.12	0.14	0.01	0.01	-0.06	-0.31	0.05	-0.10	-0.37	0.05	0.12	0.19	0.00	-0.76	-0.75	0.34	-0.44	-0.43	0.22	0.22	0.19	0.21	0.21	0.20	0.22	0.22	0.20	0.22	0.22	0.20	0.98	0.99	0.98	0.99	0.99	0.99	0.99	1.00	1.00	1.00	1.00	0.99	-0.07	0.96	0.98
PCBoom CFD ISBAP	-0.04	-0.02	-0.47	-0.12	-0.13	0.09	-0.11	-0.05	0.28	0.21	-0.17	-0.08	0.11	-0.20	0.14	0.04	0.06	-0.18	0.04	-0.20	-0.06	-0.12	-0.01	0.08	0.11	-0.03	-0.02	-0.05	-0.28	0.01	-0.10	-0.38	0.03	0.07	0.14	0.00	-0.71	-0.71	0.34	-0.38	-0.38	0.24	0.24	0.22	0.23	0.23	0.22	0.24	0.24	0.23	0.24	0.24	0.23	0.98	0.97	0.96	0.97	0.97	0.99	1.00	0.99	0.98	0.99	0.99	1.00	-0.07	0.94	0.97
PCBoom Distance	0.14	-0.04	-0.06	0.06	-0.10	-0.02	0.08	-0.06	0.09	-0.11	-0.03	0.09	-0.08	0.05	-0.07	-0.10	0.03	-0.04	0.10	0.04	0.10	0.01	0.02	0.20	0.22	0.19	-0.12	0.08	0.19	0.17	0.34	-0.12	0.02	-0.14	-0.18	0.04	0.31	0.31	-0.11	0.20	0.19	0.10	0.09	0.23	0.18	0.14	0.21	-0.03	-0.04	0.03	-0.02	-0.02	0.00	-0.09	-0.09	-0.09	-0.09	-0.09	-0.09	-0.08	-0.07	-0.07	-0.07	-0.07	-0.07	1.00	0.23	0.26
PCBoom peak pressure	0.14	-0.01	-0.48	0.08	-0.11	0.09	0.08	-0.20	0.29	-0.09	-0.07	0.07	-0.05	0.02	-0.03	-0.08	0.08	-0.08	0.09	-0.01	0.08	0.02	0.06	0.31	0.32	0.20	0.05	-0.08	-0.28	0.21	0.10	-0.43	0.05	0.14	0.19	-0.02	-0.58	-0.57	0.16	-0.37	-0.37	0.27	0.28	0.29	0.30	0.30	0.29	0.22	0.23	0.22	0.23	0.23	0.21	0.96	0.97	0.98	0.98	0.98	0.96	0.93	0.95	0.97	0.96	0.96	0.94	0.23	1.00	0.98
PCBoom CFD peak pressure	0.10	-0.02	-0.52	0.06	-0.13	0.11	0.08	-0.19	0.34	-0.04	-0.08	0.04	-0.01	-0.02	0.02	-0.06	0.09	-0.08	0.07	-0.05	0.04	0.00	0.06	0.28	0.29	0.17	0.02	-0.01	-0.22	0.19	0.13	-0.40	-0.01	0.06	0.12	0.00	-0.52	-0.51	0.18	-0.28	-0.28	0.27	0.28	0.30	0.30	0.29	0.29	0.22	0.23	0.24	0.24	0.23	0.23	0.95	0.96	0.96	0.97	0.96	0.96	0.96	0.97	0.98	0.98	0.98	0.97	0.26	0.98	1.00